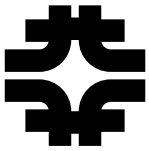

Fermi National Accelerator Laboratory

FERMILAB-Pub-97/221-T

QED Radiative Corrections to Z Boson Production and the Forward Backward Asymmetry at Hadron Colliders

U. Baur

State University of New York
Buffalo, New York 14260

S. Keller

Fermi National Accelerator Laboratory
P.O. Box 500, Batavia, Illinois 60510

W.K. Sakumoto

University of Rochester
Rochester, New York 14627

July 1997

Submitted to *Physics Letters B*

Operated by Universities Research Association Inc. under Contract No. DE-AC02-76CH03000 with the United States Department of Energy

Disclaimer

Distribution

UB-HET-97-02
FERMILAB-Pub-97/221-T
July 1997

QED Radiative Corrections to Z Boson Production and the Forward Backward Asymmetry at Hadron Colliders

U. Baur

Department of Physics, State University of New York, Buffalo, NY 14260, USA

S. Keller

Fermi National Accelerator Laboratory, Batavia, IL 60510, USA

W.K. Sakumoto

Physics Department, University of Rochester, Rochester, NY 14627, USA

Abstract

The $\mathcal{O}(\alpha)$ radiative corrections to the process $p\overset{(-)}{p} \to \gamma^*, Z \to \ell^+\ell^-$ ($\ell = e, \mu$) are calculated. Factorizing the collinear singularity associated with initial state photon bremsstrahlung into the parton distribution functions, we find that initial state corrections have a much smaller effect than final state radiative corrections. Due to mass singular logarithmic terms associated with photons emitted collinear with one of the final state leptons, QED radiative corrections strongly affect the shape of the di-lepton invariant mass distribution, the lepton transverse momentum spectrum, and the forward backward asymmetry, A_{FB}. They lead to a sizeable shift in the Z boson mass extracted from data, decrease the di-lepton cross section by up to 10%, and increase the integrated forward backward asymmetry in the Z peak region by about 7% at the Tevatron. We also investigate how experimental lepton identification requirements modify the effect of the QED corrections, and study the prospects for a high precision measurement of $\sin^2\theta_{eff}^{lept}$ using the forward backward asymmetry at the Large Hadron Collider (LHC).

Typeset using REVTEX

I. INTRODUCTION

Over the last few years, the Standard Model (SM) of electroweak interactions has been successfully tested at the one-loop level. Experiments at LEP and the SLC [1] have determined the properties of the Z boson with a precision of 0.1% or better, and correctly predicted the range of the top quark mass from loop corrections [1]. Currently, the Z boson mass is known to ± 2.0 MeV, whereas the uncertainty of the W mass, M_W, is ± 80 MeV [2]. A precise measurement of M_W and the top quark mass, m_{top}, would make it possible to derive indirect constraints on the Higgs boson mass, M_H, via top quark and Higgs boson electroweak radiative corrections to M_W [3]. With a precision of 30 MeV (10 MeV) for the W mass, and 2 GeV for the top quark mass, M_H can be predicted with an uncertainty of about 50% (20%) [4]. Comparison of these constraints on M_H with the mass obtained from direct observation of the Higgs boson in future collider experiments will be an important test of the SM.

A significant improvement in the W mass uncertainty is expected in the near future from measurements at LEP II [5] and the Fermilab Tevatron $p\bar{p}$ collider [4]. The ultimate precision expected for M_W from the combined LEP II experiments is approximately 40 MeV [5]. At the Tevatron, integrated luminosities of order 1 fb^{-1} are envisioned in the Main Injector Era, and one expects to measure the W mass with a precision of approximately 50 MeV [4] per experiment. The prospects for a precise measurement of M_W would further improve if a significant upgrade in luminosity beyond the goal of the Main Injector could be realized. With recent advances in accelerator technology [6], Tevatron collider luminosities of order $10^{33}\,\mathrm{cm}^{-2}\,\mathrm{s}^{-1}$ may become a reality, resulting in integrated luminosities of up to 10 fb^{-1} per year. With a total integrated luminosity of 30 fb^{-1}, one can target a precision of the W mass of 15 – 20 MeV [4]. A similar or better accuracy may also be reached at the Large Hadron Collider (LHC) [7].

The determination of the W mass in a hadron collider environment requires a simultaneous precision measurement of the Z boson mass, M_Z, and width, Γ_Z. When compared to

the value measured at LEP, the two quantities help to accurately determine the energy scale and resolution of the electromagnetic calorimeter, and to constrain the muon momentum resolution [8,9].

Analogous to the W mass, a very high precision measurement of the effective weak mixing angle, $\sin^2\theta_{eff}^{lept}$ [10], can be used to extract information on the Higgs boson mass [4,11]. At hadron colliders, the effective weak mixing angle can be determined from the forward backward asymmetry, A_{FB}, in di-lepton production in the vicinity of the Z pole [12].

In order to measure A_{FB} and the Z boson mass with high precision in a hadron collider environment, it is necessary to fully understand and control higher order QCD and electroweak corrections. A complete calculation of the full $\mathcal{O}(\alpha)$ radiative corrections to $p\overset{(-)}{p} \to \gamma^*, Z \to \ell^+\ell^-$ has not been carried out yet. In a previous calculation, only the final state photonic corrections had been included [13,14], using an approximation in which the sum of the soft and virtual part is indirectly estimated from the inclusive $\mathcal{O}(\alpha^2)$ $Z \to \ell^+\ell^-(\gamma)$ width and the hard photon bremsstrahlung contribution.

In this paper, we present a more complete calculation of the $\mathcal{O}(\alpha)$ QED corrections to $p\overset{(-)}{p} \to \gamma^*, Z \to \ell^+\ell^-$. Real and virtual initial and final state corrections, as well as the interference between initial and final state corrections are included. Purely weak corrections are expected to be very small and are therefore ignored. Our calculation also takes into account the mass of the final state leptons, which regularizes the collinear singularity associated with final state photon radiation. Both Z and photon exchange diagrams with all $\gamma - Z$ interference effects are incorporated. The di-lepton invariant mass thus is *not* restricted to the Z peak region. Low mass Drell-Yan production is of interest because of the sensitivity to parton distribution functions (PDF's) at small x values [15]. High mass lepton pairs and the forward backward asymmetry above the Z peak [16] can be used to search for additional neutral vector bosons, and to constrain their couplings [17,18]. Results from our calculation have been used in Ref. [18] to compare experimental data with the SM prediction for A_{FB}.

To perform our calculation, we use the Monte Carlo method for next-to-leading-order (NLO) calculations described in Ref. [19]. The matrix elements for radiative Z production

and decay are taken from Ref. [20] and [21]. With the Monte Carlo method, it is easy to calculate a variety of observables simultaneously and to simulate detector response. Special care has to be taken in calculating the radiative corrections associated with photon radiation from the incoming quarks and antiquarks. In the parton model, quarks are assumed to be massless, and initial state photon radiation results in collinear singularities. The singular terms are universal to all orders in perturbation theory and can be removed by universal collinear counterterms generated by 'renormalizing' the parton distribution functions [22,23], in complete analogy to gluon emission in QCD. A calculation of QED corrections using definite, non-zero, values for quark masses [24] and not factorizing the corresponding collinear logarithms leads to a considerable overestimation of the effects of initial state photon corrections. However, QED corrections to the evolution of the parton distribution functions are not included in our calculation; a complete fit of the PDF's including all QED effects is beyond the scope of this paper. The technical details of our calculation are described in Sec. II.

Numerical results for $p\bar{p}$ collisions at $\sqrt{s} = 1.8$ TeV are presented in Sec. III. Due to the mass singular logarithms associated with final state photon bremsstrahlung in the limit where the photon is emitted collinear with one of the charged leptons, the di-lepton invariant mass distribution is strongly affected by QED corrections, in particular in the vicinity of the Z boson resonance. As a result, the value extracted for M_Z from data is shifted to a lower value. The amount of the shift depends on the lepton mass, and the detector resolution [8,9]. QED radiative corrections also significantly affect the Z boson production cross section when cuts are imposed, the transverse momentum distribution of the leptons, and the forward backward asymmetry below the Z pole. For di-lepton masses between 50 GeV and 100 GeV, the final state $\mathcal{O}(\alpha)$ QED corrections are larger than the $\mathcal{O}(\alpha_s)$ QCD corrections.

In Sec. III, using a simplified model of the CDF detector as an example, we also investigate how the finite energy and momentum resolution of realistic detectors affect the QED corrections. Electrons and photons which are almost collinear are difficult to discriminate,

and the momenta of the two particles are thus recombined into an effective electron momentum [8,9] if they traverse the same calorimeter cell, or, alternatively, if their separation in the pseudorapidity – azimuthal angle plane is below a critical value. The second procedure completely eliminates the mass singular logarithms. With the first method, residual effects of these terms remain when both particles are almost collinear, but hit different calorimeter cells. In practice, the numerical difference between the two procedures is moderate; in both cases the significance of the QED corrections is considerably reduced. In contrast, photons which are almost collinear with muons are rejected if they are too energetic [8] which results in residual logarithmic corrections to observable quantities in $\mu^+\mu^-$ production. Transverse momentum and rapidity cuts are found to affect the lepton pair invariant mass distribution and forward backward asymmetry in a similar way at the Born level and at $\mathcal{O}(\alpha^3)$.

Recently, it has been suggested [11], that an ultra precise measurement of $\sin^2\theta_{eff}^{lept}$ may be possible at the LHC (pp collisions at $\sqrt{s} = 14$ TeV [25]) in the muon channel, using the forward backward asymmetry in the Z peak region. At the LHC, the forward backward asymmetry is significantly reduced compared to the Tevatron because of the larger sea – sea quark parton flux. We find that the sensitivity of A_{FB} to the effective weak mixing angle strongly depends on the rapidity range over which the leptons can be detected. The forward backward asymmetry at the LHC, including $\mathcal{O}(\alpha)$ QED and $\mathcal{O}(\alpha_s)$ QCD corrections, is studied in detail in Sec. IV. Finally, our conclusions are presented in Sec. V.

II. METHOD OF CALCULATION

The calculation presented here employs a combination of analytic and Monte Carlo integration techniques. Details of the method can be found in Ref. [19]. The calculation of di-lepton production in hadronic collisions at $\mathcal{O}(\alpha^3)$ includes contributions from the square of the Born graphs, the interference between the Born diagrams and the virtual one loop graphs, and the square of the real emission diagrams which we adopt from Refs. [20,21]. The diagrams contributing to the $\mathcal{O}(\alpha)$ QED corrections can be separated into gauge invariant

subsets corresponding to initial and final state corrections. The squared matrix element for the real emission diagrams is then given by

$$|\mathcal{M}^{2\to 3}|^2 = |\mathcal{M}_i^{2\to 3}|^2 + 2Re[\mathcal{M}_i^{2\to 3}(\mathcal{M}_f^{2\to 3})^*] + |\mathcal{M}_f^{2\to 3}|^2. \tag{1}$$

$\mathcal{M}_i^{2\to 3}$ and $\mathcal{M}_f^{2\to 3}$ are the separately gauge invariant matrix elements associated with initial and final state radiation.

The basic idea of the method employed here is to isolate the soft and collinear singularities associated with the real photon emission subprocesses by partitioning phase space into soft, collinear, and finite regions. This is done by introducing theoretical soft and collinear cutoff parameters, δ_s and δ_c. Using dimensional regularization [26], the soft and collinear singularities are exposed as poles in ϵ (the number of space-time dimensions is $N = 4 - 2\epsilon$ with ϵ a small number). In the soft and collinear regions the cross section is proportional to the Born cross section. The soft region is defined by requiring that the photon energy in the $q\bar{q}$ center of mass frame, E_γ, is $E_\gamma < \delta_s\sqrt{\hat{s}}/2$ ($\hat{s}$ denotes the squared parton center of mass energy). We can then evaluate, in N dimensions, the $2 \to 3$ diagrams using the soft photon approximation, where the photon momentum is set to zero in the numerator, and integrate over the soft region. The soft singularities originating from final state photon radiation cancel against the corresponding singularities from the interference of Born and final state virtual corrections. Similarly, the soft singularities associated with initial state photon emission and interference effects between initial and final state radiation cancel against the corresponding singularities originating from initial state vertex corrections, and the $Z\gamma$ and $\gamma\gamma$ box diagrams, respectively. The remainder is then evaluated via Monte Carlo integration as part of the $2 \to 2$ contribution. For $E_\gamma > \delta_s\sqrt{\hat{s}}/2$, the real photon emission diagrams are calculated in four dimensions [20,21] using standard three body phase space Monte Carlo integration techniques.

The collinear singularity associated with photon radiation from the final state lepton line is regulated by the finite lepton mass. The collinear singularities originating from initial state photon bremsstrahlung are universal to all orders of perturbation theory and

can be cancelled by universal collinear counterterms generated by renormalizing the parton distribution functions [22,23], in complete analogy to gluon emission in QCD [27]. They occur when the final state photon and the partons in the initial state are collinear so that denominators of propagators such as

$$\hat{t} = -2p_{\bar{q}} \cdot p_\gamma \tag{2}$$

and

$$\hat{u} = -2p_q \cdot p_\gamma \tag{3}$$

vanish. Here, p_q ($p_{\bar{q}}$) denotes the quark (anti-quark), and p_γ the photon four momentum vector. Only $|\mathcal{M}_i^{2\to3}|^2$ is divergent in the collinear limit; the initial – final state interference term, $Re[\mathcal{M}_i^{2\to3}(\mathcal{M}_f^{2\to3})^*]$ exhibits only soft singularities for massive final state leptons. In the collinear region, $|\hat{t}|$, $|\hat{u}| < \delta_c\hat{s}$, $|\mathcal{M}_i^{2\to3}|^2$ is evaluated in the leading pole approximation. After N-dimensional integration over the photon phase space variables, the explicit singularity can be factorized into the parton distribution functions. The remainder is evaluated as part of the $2 \to 2$ contribution. If $|\hat{t}|$, $|\hat{u}| > \delta_c\hat{s}$, the $2 \to 3$ diagrams are again evaluated numerically in four dimensions using the full three body phase space.

In order to treat the $\mathcal{O}(\alpha)$ initial state QED corrections to di-lepton production in hadronic collisions in a consistent way, QED corrections should be incorporated in the global fitting of the PDF's. Current fits [28] to the PDF's do not include QED corrections. A study of the effect of QED corrections on the evolution of the parton distribution functions indicates [22] that the modification of the PDF's is small. We have not attempted to include QED corrections to the PDF evolution in the calculation presented here. The missing QED corrections to the PDF introduce an uncertainty which, however, probably is much smaller than the present uncertainties on the parton distribution functions.

Absorbing the collinear singularity into the PDF's introduces a QED factorization scheme dependence. The squared matrix elements for different QED factorization schemes differ by the finite $\mathcal{O}(\alpha)$ terms which are absorbed into the PDF's in addition to the singular terms.

As long as QED corrections to the PDF evolution are not included, the $\mathcal{O}(\alpha^3)$ cross section will depend on the QED factorization scheme used. We have performed our calculation in the QED $\overline{\rm MS}$ and DIS schemes, which are defined analogously to the usual $\overline{\rm MS}$ [29] and DIS [30] schemes used in QCD calculations. Unless noted otherwise, we will use the QED DIS scheme which minimizes the effect of the $\mathcal{O}(\alpha)$ QED corrections on the PDF by requiring the same expression for the leading and next-to-leading order structure function F_2 in deep inelastic scattering.

The $2 \to 2$ contribution associated with initial state radiative (ISR) corrections, including the correction terms originating from the absorption of the initial state collinear singularity, can be obtained from the corresponding $\mathcal{O}(\alpha_s)$ QCD corrections [31] by replacing $(4/3)\alpha_s$ by αQ_q^2, where Q_q is the electric charge of the quark in units of the proton charge, in all relevant matrix element and cross section formulae. The $2 \to 2$ contribution induced by the soft and virtual final state radiative (FSR) corrections is given by:

$$\Delta|\mathcal{M}^{2\to 2}|^2_f = |\mathcal{M}^{Born}|^2 \left[2\,\frac{\alpha}{\pi}\left(\log\frac{\hat{s}}{m_\ell^2} - 1\right)\log(\delta_s) + 2\,\frac{\alpha}{\pi}\left(\frac{3}{4}\log\frac{\hat{s}}{m_\ell^2} + \frac{\pi^2}{6} - 1\right) + \mathcal{O}(\delta_s)\right] \quad (4)$$

where m_ℓ is the lepton mass and

$$\mathcal{M}^{Born} = \mathcal{M}^\gamma + \mathcal{M}^Z \quad (5)$$

is the Born $q\bar{q} \to \gamma^*,\, Z \to \ell^+\ell^-$ matrix element. Finally, the $2 \to 2$ contribution induced by the $\mathcal{O}(\alpha^3)$ initial – final state interference correction terms is given by

$$\begin{aligned}
\Delta|\mathcal{M}^{2\to 2}|^2_{int} = & -2Q_q\,\frac{\alpha}{\pi}\,\beta_{int}\log(\delta_s)\,|\mathcal{M}^\gamma|^2 \\
& -2Q_q\,\frac{\alpha}{\pi}\,\beta_{int}\,Re\left[\mathcal{M}^\gamma\mathcal{M}^{Z*}\log\left(\frac{\hat{s}\delta_s^2}{M_Z^2 - \hat{s} - i\hat{s}\gamma_Z}\right)\right] \\
& -2Q_q\,\frac{\alpha}{\pi}\,\beta_{int}\,\log\left|\frac{\hat{s}\delta_s}{M_Z^2 - \hat{s} - i\hat{s}\gamma_Z}\right|\,|\mathcal{M}^Z|^2 \\
& + \text{finite } \gamma\gamma \text{ and } \gamma Z \text{ box terms}
\end{aligned} \quad (6)$$

with

$$\beta_{int} = \log\left(\frac{\hat{t}_1}{\hat{u}_1}\right) \quad (7)$$

and

$$\gamma_Z = \frac{, Z}{M_Z}. \tag{8}$$

In our calculation, we use the full $\hat{s}$ dependent width in the Z boson propagator. The $\hat{t}_1$ and $\hat{u}_1$ are Mandelstam variables of the $2 \to 2$ reaction:

$$\hat{t}_1 = -2p_q \cdot p_{\ell^+}, \tag{9}$$

$$\hat{u}_1 = -2p_q \cdot p_{\ell^-}. \tag{10}$$

The finite terms from the $\gamma\gamma$ and γZ box diagrams are identical to those in $e^+e^- \to q\bar{q}$ and can be found in Refs. [32] and [33].

The end result of the calculation consists of two sets of weighted events corresponding to the $2 \to 2$ and $2 \to 3$ contributions. Each set depends on the parameters δ_s and δ_c. The sum of the two contributions, however, must be independent of δ_s and δ_c, as long as the two parameters are taken small enough so that the approximations used are valid. In Figs. 1 and 2 we show the dependence of the $p\bar{p} \to \ell^+\ell^-(\gamma)$ cross section in the Z peak region (75 GeV $< m(\ell^+\ell^-) <$ 105 GeV) on δ_s and δ_c; $m(\ell^+\ell^-)$ denotes the di-lepton invariant mass. To compute the cross section, we use here and in all subsequent figures the MRSA set of parton distribution functions [34], and take the renormalization scale μ and the QED and QCD factorization scales, M_{QED} and M_{QCD}, to be $\mu^2 = M^2_{QED} = M^2_{QCD} = \hat{s}$.

Figure 1 displays the cross section as a function of δ_c (Fig. 1a) and δ_s (Fig. 1b) for initial state radiative corrections only. In order to exhibit the independence of the cross section from the parameters δ_s and δ_c more clearly, we have not included the Born cross section in the $2 \to 2$ contribution. The ISR corrections to the cross section for electron and muon final states are virtually identical. While the separate $2 \to 2$ and $2 \to 3$ $\mathcal{O}(\alpha)$ contributions vary strongly with δ_s and δ_c, the sum is independent of the two parameters within the accuracy of the Monte Carlo integration. The total contribution of initial state radiation diagrams to the total cross section in the Z pole region is found to be about 0.43% of the Born cross section for the parameters chosen. In the QED $\overline{\rm MS}$ scheme, the contribution of the ISR diagrams

is about 10% smaller than in the QED DIS scheme. QED corrections to the PDF's and purely weak one loop corrections to the matrix elements, both which are not included in our calculation, are expected to be of the same order of magnitude.

In Fig. 2, we show the $p\bar{p} \to \ell^+\ell^-(\gamma)$ cross section in the Z peak region (75 GeV $< m(\ell^+\ell^-) <$ 105 GeV) as a function of the soft cutoff parameter δ_s for electron and muon final states for FSR corrections. Radiation of photons collinear with one of the leptons gives rise to terms proportional to $\log(\hat{s}/m_\ell^2)\log(\delta_s)$ (see Eq. (4)) in both the $2 \to 2$ and $2 \to 3$ contributions. As demonstrated in Fig. 2, these terms cancel and the total cross section is independent of δ_s. Due to the smaller mass of the electron, the variation of the $2 \to 2$ and $2 \to 3$ contributions with δ_s is more pronounced in the electron case. The solid line in Fig. 2 indicates the cross section in the Born approximation. The total $\mathcal{O}(\alpha^3)$ cross section in the $e^+e^-(\gamma)$ ($\mu^+\mu^-(\gamma)$) case is found to be about 7% (3%) smaller than the Born cross section. The difference in the NLO $e^+e^-(\gamma)$ and $\mu^+\mu^-(\gamma)$ cross section can be traced to residual logarithmic correction terms which arise from the finite lepton pair invariant mass range considered in Fig. 2 (see Sec. IIIA). If the integration would be carried out over the full range $m(\ell^+\ell^-) > 2m_\ell$, these terms would vanish [35]. From Fig. 2 one also observes that, due to the residual logarithmic terms, final state radiation effects are much larger than those which originate from initial state radiation. The $2 \to 2$ and the $2 \to 3$ contributions to the FSR corrections each are trivially independent of the collinear cutoff δ_c.

Similar to the FSR corrections, one can show that the sum of the $2 \to 2$ and $2 \to 3$ contributions of the initial – final state interference terms is independent of δ_s. The interference terms are typically of the same size as the initial state corrections.

The missing QED corrections to the PDF's create a dependence of the $\mathcal{O}(\alpha)$ initial state corrections on the factorization scale M_{QED} which is stronger than that of lowest order calculation. On the other hand, final state and initial – final state interference terms depend on the factorization scale only through the PDF's. These terms therefore exhibit a sensitivity to the factorization scale which is similar to that of the lowest order calculation. Since the Born cross section and final state corrections are much larger than corrections from initial

state radiation, the scale dependence of the complete $\mathcal{O}(\alpha^3)$ cross section is similar to that of the Born cross section.

In conclusion, in Figs. 1 and 2 we demonstrated that the $p\overset{(-)}{p} \to \gamma^*, Z \to \ell^+\ell^-(\gamma)$, cross section for 75 GeV $< m(\ell^+\ell^-) <$ 105 GeV is independent of the soft and collinear cutoff parameters δ_s and δ_c within the accuracy of the Monte Carlo integration. Independence of the cross section from these two parameters can also be demonstrated for lepton pair invariant masses below ($m(\ell^+\ell^-) < 75$ GeV) and above ($m(\ell^+\ell^-) > 105$ GeV) the Z peak. In the following, the soft and collinear cutoff parameters will be fixed to $\delta_s = 10^{-2}$ and $\delta_c = 10^{-3}$, unless explicitly stated otherwise.

III. $\mathcal{O}(\alpha)$ CORRECTIONS TO DI-LEPTON PRODUCTION AT THE TEVATRON

We shall now discuss the phenomenological implications of $\mathcal{O}(\alpha)$ QED corrections to di-lepton production at the Tevatron ($p\bar{p}$ collisions at $\sqrt{s} = 1.8$ TeV). We first discuss the impact of QED corrections on the lepton pair invariant mass distribution and the forward backward asymmetry. We then consider how the finite resolution of detectors and experimental lepton identification requirements modify the effects of the QED corrections, and investigate how $\mathcal{O}(\alpha)$ QED corrections affect the measured di-lepton (Z boson) cross section within the cuts imposed. Finally, we study the effect of the full radiative corrections on the Z boson mass extracted from data. The SM parameters used in our numerical simulations are $M_Z = 91.187$ GeV, $\alpha(M_Z^2) = 1/128$, $, _Z = 2.50$ GeV and $\sin^2\theta_{eff}^{lept} = 0.2319$. These values are consistent with recent measurements at LEP, SLC and the Tevatron [1].

A. QED Corrections to the Di-lepton Invariant Mass Distribution and A_{FB}

As we pointed out in Sec. II, final state photon radiation leads to corrections which are proportional to $\alpha \log(\hat{s}/m_\ell^2)$. These terms are large, and are expected to significantly influence the shape of the di-lepton invariant mass distribution. The $\mathcal{O}(\alpha^3)$ $\ell^+\ell^-$ invariant mass distribution in the vicinity of the Z peak for the electron (solid line) and muon case

(dotted line) is shown in Fig. 3 together with the lowest order prediction (dashed line). No detector resolution effects or acceptance cuts are taken into account in any of the figures shown in this subsection. QED corrections decrease (increase) the cross section at (below) the peak. At the peak position, the differential cross section is reduced by a factor [36]

$$\rho \approx 1 + \beta \log\left(\frac{\gamma Z}{M_Z}\right) \tag{11}$$

with

$$\beta = \frac{2\alpha}{\pi}\left(\log\frac{M_Z^2}{m_\ell^2} - 1\right), \tag{12}$$

i.e. by about 30% in the electron case and by about 20% in the muon case. The shape of the Z boson resonance curve is seen to be considerably distorted by the $\mathcal{O}(\alpha)$ QED corrections. Photon radiation from one of the leptons lowers the di-lepton invariant mass. Events from the Z peak region therefore are shifted towards smaller values of $m(\ell^+\ell^-)$, thus reducing the cross section in and above the peak region, and increasing the rate below the Z pole. Due to the $\log(\hat{s}/m_\ell^2)$ factor, the effect of the corrections is larger in the electron case. The lowest order cross section is almost indistinguishable for the two lepton flavors.

The size of the QED corrections to lepton pair production at the Tevatron becomes more apparent in Fig. 4 where we display the ratio of the $\mathcal{O}(\alpha^3)$ and the Born cross section as a function of the lepton pair invariant mass. For 40 GeV $< m(\ell^+\ell^-) <$ 110 GeV, the cross section ratio is seen to vary rapidly. Below the Z peak, QED corrections enhance the cross section by up to a factor 2.7 (1.9) for electrons (muons). The maximum enhancement of the cross section occurs at $m(\ell^+\ell^-) \approx 75$ GeV. For $m(\ell^+\ell^-) < 40$ GeV ($m(\ell^+\ell^-) > 130$ GeV), $\mathcal{O}(\alpha)$ QED corrections uniformly reduce the differential cross section by about 7% (12%) in the electron case, and $\approx 2.5\%$ ($\approx 7\%$) in the muon case. Integrating over the full di-lepton invariant mass region, the large positive and negative corrections below and above M_Z cancel [35]. For 40 GeV$< m(\ell^+\ell^-) < M_Z$, a large fraction of events contains a photon with energy $E_\gamma > 1$ GeV. As we have stated before, the dominant QED radiative corrections are proportional to $\log(\hat{s}/m_\ell^2)$. The $p\bar{p} \to \mu^+\mu^-$ cross section is therefore less affected by radiative corrections than the $p\bar{p} \to e^+e^-$ rate.

It should be emphasized that the enhanced significance of the $\mathcal{O}(\alpha)$ QED corrections below the Z peak is a direct consequence of the Breit-Wigner resonance of the Z boson. The $\mathcal{O}(\alpha^2)$ radiative corrections therefore should be a factor $\mathcal{O}((\alpha/\pi)\log(\hat{s}/m_\ell^2))$ smaller than the $\mathcal{O}(\alpha)$ corrections. The effect of higher order QED corrections on the $m(\ell^+\ell^-)$ distribution can be estimated using the fragmentation function approach of Ref. [37]. In this approach, the radiatively corrected cross section is obtained by convoluting the lowest order di-lepton cross section with a radiator function, which to all order sums the dominant and non-dominant logarithmic terms. Figure 5 displays the ratio of the $\mathcal{O}(\alpha^3)$ cross section and the cross section in the fragmentation function approach as a function of $m(\ell^+\ell^-)$. Only final state corrections are taken into account in the fragmentation function approach. As for the $\mathcal{O}(\alpha)$ corrections, initial state radiation contributions are expected to be small and, therefore, are ignored. Figure 5 shows that higher order final state QED corrections reduce the effect of the $\mathcal{O}(\alpha)$ corrections and are indeed of the size naively expected. In the Z peak region, the higher order final state corrections vary rapidly with $m(\ell^+\ell^-)$ and change the differential cross section by up to 10% (3%) in the electron (muon) case.

In Fig. 6, we compare the impact of the full $\mathcal{O}(\alpha)$ QED corrections (solid line) on the muon pair invariant mass spectrum with that of final state (dashed line) and initial state radiative corrections (dotted line) only. Qualitatively similar results are obtained in the electron case. Final state radiative corrections are seen to completely dominate over the entire mass range considered. They are responsible for the strong modification of the di-lepton invariant mass distribution. In contrast, initial state corrections are uniform and small ($\approx +0.4\%$).

At small di-lepton invariant masses, photon exchange dominates and the initial – final state interference terms are almost completely antisymmetric in $\cos\bar{\theta}^*$ [32,33,38], where $\bar{\theta}^*$ is the lepton scattering angle in the parton center of mass frame. The contribution of these interference terms to the di-lepton invariant mass distribution is extremely small (0.01% – 0.1%) for $m(\ell^+\ell^-) < M_Z$. For values of $m(\ell^+\ell^-)$ sufficiently above the Z mass, initial – final state interference terms reduce the $\mathcal{O}(\alpha^3)$ cross section by about 1%.

Next-to-leading order QCD corrections to lepton pair production in $p\bar{p}$ collisions at Tevatron energies are known [31] to enhance the cross section by about 16% – 25%. Since these are initial state corrections, the NLO QCD to leading order cross section ratio varies only slowly with the di-lepton invariant mass, similar to what we found for initial state QED corrections. Comparing the size of the $\mathcal{O}(\alpha)$ QED and $\mathcal{O}(\alpha_s)$ QCD corrections, one observes that they are of similar magnitude above the Z peak, but have opposite sign. In the invariant mass range between 50 GeV and 100 GeV, QED corrections are significantly larger than those induced by the strong interactions. The relative importance of the QED corrections is due to the combined effect of mass singular logarithms associated with final state photon radiation, and the Z boson Breit-Wigner resonance.

Since QED corrections strongly affect the shape of the lepton pair invariant mass distribution below the Z peak, one expects that they may also have a significant impact on other observables in this region. In Fig. 7, we show the forward backward asymmetry, A_{FB}, as a function of the lepton pair invariant mass in the Born approximation (dashed line), and including $\mathcal{O}(\alpha)$ QED corrections for electron (solid line) and muon final states (dotted line). Here, A_{FB} is defined by

$$A_{FB} = \frac{F - B}{F + B} \tag{13}$$

where

$$F = \int_0^1 \frac{d\sigma}{d\cos\theta^*} d\cos\theta^*, \qquad B = \int_{-1}^0 \frac{d\sigma}{d\cos\theta^*} d\cos\theta^*. \tag{14}$$

$\cos\theta^*$ is given by [18,39]

$$\cos\theta^* = \frac{2}{m(\ell^+\ell^-)\sqrt{m^2(\ell^+\ell^-) + p_T^2(\ell^+\ell^-)}} \left[p^+(\ell^-)p^-(\ell^+) - p^-(\ell^-)p^+(\ell^+)\right] \tag{15}$$

with

$$p^\pm = \frac{1}{\sqrt{2}}(E \pm p_z), \tag{16}$$

where E is the energy and p_z is the longitudinal component of the momentum vector. In this definition of $\cos\theta^*$, the polar axis is taken to be the bisector of the proton beam momentum

and the negative of the anti-proton beam momentum when they are boosted into the $\ell^+\ell^-$ rest frame. In $p\bar{p}$ collisions at Tevatron energies, the flight direction of the incoming quark coincides with the proton beam direction for a large fraction of the events. The definition of $\cos\theta^*$ in Eq. (15) has the advantage of minimizing the effects of the QCD corrections (see below). In the limit of vanishing di-lepton p_T, θ^* coincides with the angle between the lepton and the incoming proton in the $\ell^+\ell^-$ rest frame.

Our result for A_{FB} in the Born approximation agrees with that presented in Ref. [16]. As expected, the $\mathcal{O}(\alpha)$ QED corrections to A_{FB} are large in the region below the Z peak. Since events from the Z peak, where A_{FB} is positive and small, are shifted towards smaller values of $m(\ell^+\ell^-)$ by photon radiation, the forward backward asymmetry is significantly reduced in magnitude by radiative corrections for 50 GeV $< m(\ell^+\ell^-) <$ 90 GeV.

The forward backward asymmetry in the Born approximation is small at low di-lepton masses, because of the dominance of photon exchange and the vectorlike coupling of the photon to leptons. For di-lepton masses below 40 GeV, the $\mathcal{O}(\alpha)$ initial – final state interference correction terms are almost completely antisymmetric in $\cos\theta^*$ and comprise the most important component of the QED corrections to A_{FB}. In this region, the $\mathcal{O}(\alpha)$ QED corrections to A_{FB} are therefore large. Initial – final state interference terms do not contain any mass singular contributions. As a result, the forward backward asymmetries for electron and muon final states are similar for $m(\ell^+\ell^-) < 40$ GeV. Details of the asymmetry in the low di-lepton mass region are shown in the inset of Fig. 7. Effects from purely weak corrections are not included in our calculation. They could have a non-negligible effect on the forward backward asymmetry at low di-lepton masses, similar to the situation encountered in $e^+e^- \to \mu^+\mu^-$ [40].

In contrast to the lepton pair invariant mass distribution, QED corrections to A_{FB} are small for $m(\ell^+\ell^-) > 120$ GeV. They reduce the forward backward asymmetry by about 1% in this region. Initial and final state corrections to A_{FB} are of similar size for lepton pair invariant masses above the Z peak.

Recently, the CDF Collaboration has presented a first measurement of the integrated

forward backward asymmetry in $p\bar{p} \to e^+e^-X$ at the Tevatron for $m(e^+e^-) > 105$ GeV, together with a more refined measurement in the Z peak region (75 GeV $< m(e^+e^-) <$ 105 GeV) [18]. In Table I, we list the experimental values, together with the theoretical prediction with and without $\mathcal{O}(\alpha)$ QED corrections. QED corrections are seen to increase the asymmetry by about 8% in the peak region. In the muon channel, the increase in A_{FB} for 75 GeV $< m(\mu^+\mu^-) <$ 105 GeV due to radiative corrections is approximately 4%.

In the Z peak region, A_{FB} provides a tool to measure $\sin^2\theta_{eff}^{lept}$ [12]. For 75 GeV $< m(\ell^+\ell^-) <$ 105 GeV and $\sqrt{s} = 1.8$ TeV, the forward backward asymmetry can to a very good approximation be parameterized by [16]

$$A_{FB} = b\left(a - \sin^2\theta_{eff}^{lept}\right) \tag{17}$$

both in the Born approximation and including $\mathcal{O}(\alpha)$ QED corrections. For the parameters a and b we find in the Born approximation

$$a^{\rm Born} = 0.2454, \qquad b^{\rm Born} = 3.6 \tag{18}$$

for e^+e^- as well as $\mu^+\mu^-$ final states, and

$$a^{\mathcal{O}(\alpha^3)} = a^{\rm Born} + \Delta a^{\rm QED}, \qquad b^{\mathcal{O}(\alpha^3)} = b^{\rm Born} + \Delta b^{\rm QED} \tag{19}$$

with

$$\Delta a^{\rm QED} \approx 0.0010, \qquad \Delta b^{\rm QED} \approx 0 \tag{20}$$

for $p\bar{p} \to e^+e^-(\gamma)$, and

$$\Delta a^{\rm QED} \approx 0.0006, \qquad \Delta b^{\rm QED} \approx -0.3 \tag{21}$$

for $p\bar{p} \to \mu^+\mu^-(\gamma)$. The change of the effective weak mixing angle due to QED radiative corrections is a factor 3 to 4 larger than the current experimental uncertainty, $\delta\sin^2\theta_{eff}^{lept} = 0.00024$ [1].

In Ref. [12], the approximation used to estimate the electroweak corrections to A_{FB} resulted in a significant dependence of the correction to $\sin^2\theta_{eff}^{lept}$ on the infrared cutoff

used in the calculation. In contrast, as explained in detail in Sec. II, our results are cutoff independent. This will make it possible to substantially reduce the theoretical uncertainty of the weak mixing angle extracted from future measurements of A_{FB} at the Tevatron.

B. Aspects of Experimental Lepton Identification and QED Radiative Corrections

It is well-known [35] that the mass singular logarithmic terms which appear in higher orders of perturbation theory are eliminated when inclusive observables are considered. As explained below, the finite resolution of detectors prevents fully exclusive measurements. Detector effects, which we have completely ignored so far, therefore may significantly modify the effect of QED radiative corrections. To simulate detector acceptance, we impose the following transverse momentum (p_T) and pseudo-rapidity (η) cuts:

electrons	muons
$p_T(e) > 20$ GeV	$p_T(\mu) > 25$ GeV
$\lvert\eta(e)\rvert < 2.4$	$\lvert\eta(\mu)\rvert < 1.0$

In addition, we require that at least one electron (muon) is in the central part of the detector: $|\eta(e)| < 1.1$ ($|\eta(\mu)| < 0.6$). These cuts approximately model the acceptance of the CDF detector for electrons and muons. Uncertainties in the energy measurements of the charged leptons in the detector are simulated in the calculation by Gaussian smearing of the particle four-momentum vector with standard deviation σ which depends on the particle type and the detector. The numerical results presented here were calculated using σ values based on the CDF [41] specifications. Similar results are obtained if the acceptances and energy resolutions of the DØ detector are used [9].

The granularity of the detectors and the size of the electromagnetic showers in the calorimeter make it difficult to discriminate between electrons and photons with a small opening angle. We therefore recombine the four-momentum vectors of the electron and photon to an effective electron four-momentum vector if both traverse the same calorimeter cell, assuming a calorimeter segmentation of $\Delta\eta \times \Delta\phi = 0.1 \times 15^\circ$ (ϕ is the azimuthal angle

in the transverse plane). This procedure is similar to that used by the CDF Collaboration. The segmentation chosen corresponds to that of the central part of the CDF calorimeter [8]. The DØ Collaboration uses a slightly different recombination procedure where the electron and photon four-momentum vectors are combined if their separation in the pseudorapidity – azimuthal angle plane, $\Delta R(e,\gamma) = \sqrt{(\Delta\eta(e,\gamma))^2 + (\Delta\phi(e,\gamma))^2}$, is smaller than a critical value, R_c. For $R_c = 0.2$ [9], the numerical results obtained are similar to those found with the calorimeter segmentation we use (see above).

Muons are identified in a hadron collider detector by hits in the muon chambers. In addition, one requires that the associated track is consistent with a minimum ionizing particle. This limits the energy of a photon which traverses the same calorimeter cell as the muon to be smaller than a critical value E_c^γ. In the subsequent discussion, we assume $E_c^\gamma = 2$ GeV [8].

In Fig. 8a (Fig. 8b) we show how detector effects change the ratio of the $\mathcal{O}(\alpha^3)$ to leading order differential cross sections as a function of the e^+e^- ($\mu^+\mu^-$) invariant mass. The finite energy resolution and the acceptance cuts have only a small effect on the cross section ratio. The lepton identification criteria, on the other hand, are found to have a large impact. Recombining the electron and photon four-momentum vectors if they traverse the same calorimeter cell greatly reduces the effect of the mass singular logarithmic terms. These terms survive only in the rare case when both particles are almost collinear, but hit different calorimeter cells[1]. Although the recombination of the electron and photon momenta reduces effect of the $\mathcal{O}(\alpha)$ QED corrections, the remaining corrections are still sizeable. Below (at) the Z peak, they enhance (suppress) the lowest order differential cross section by up to a factor 1.6 (0.9) [see Fig. 8a]. For $m(e^+e^-) \gg M_Z$, the magnitude of the QED corrections is reduced from approximately 12% to 5%.

---

[1]In the case where the four-momentum vectors of the two particles are recombined for $\Delta R(e,\gamma) < R_c$, the mass singular terms are entirely eliminated, and the lepton mass in the logarithmic terms is replaced by the minimum $e\gamma$ invariant mass.

For muon final states (see Fig. 8b), the requirement of $E_\gamma < E_c^\gamma = 2$ GeV for a photon which traverses the same calorimeter cell as the muon reduces the hard photon part of the $\mathcal{O}(\alpha^3)$ $\mu^+\mu^-(\gamma)$ cross section. As a result, the magnitude of the QED corrections below the Z peak is reduced. At the Z pole the corrections remain unchanged, and for $\mu^+\mu^-$ masses larger than M_Z they become more pronounced. For $m(\mu^+\mu^-) > 120$ GeV, QED corrections reduce the $\mu^+\mu^-$ cross section by 12% to 14%.

We would like to emphasize that the survival of mass singular terms in certain cases does not contradict the KLN theorem [35]. The KLN theorem requires that mass singular logarithmic terms which appear in higher orders of perturbation theory are eliminated when inclusive observables are considered. Recombining the lepton and photon momenta for small opening angles an inclusive quantity is formed, and the mass singular logarithmic terms are eliminated in the reconstructed $\ell^+\ell^-$ invariant mass distribution. On the other hand, if the lepton and photon momenta are not combined, one performs an exclusive measurement, the KLN theorem does not apply, and logarithmic terms remain present in the measured di-lepton invariant mass distribution.

It should be noted that the differential cross section ratio shown in Fig. 8 becomes ill defined in the threshold region $m(\ell^+\ell^-) \approx 2p_T^{cut}(\ell)$, where $p_T^{cut}(\ell)$ is the charged lepton p_T threshold. For $m(\ell^+\ell^-) \leq 2p_T^{cut}(\ell)$, the Born cross section vanishes, and the cross section ratio is undefined. The $\mathcal{O}(\alpha^3)$ cross section is small, but non-zero, in this region. The largest contribution to the cross section for $m(\ell^+\ell^-) \leq 2p_T^{cut}(\ell)$ originates from initial state radiation configurations, where the leptons have a small relative opening angle and are balanced by a high p_T photon in the opposite hemisphere. Close to the threshold, $m(\ell^+\ell^-) \approx 2p_T^{cut}(\ell)$, large logarithmic corrections are present, and for an accurate prediction of the cross section those corrections need to be resummed. The results of Fig. 8 in this region should therefore be interpreted with caution. Similar conclusions can also be drawn for the forward backward asymmetry in the threshold region.

In Fig. 9, we show how detector effects affect the forward backward asymmetry for electron (Fig. 9a) and muon final states (Fig. 9b). In addition to the cuts listed at the

beginning of this subsection, we require [18]

$$|\cos\theta^*| < 0.8. \tag{22}$$

For comparison, we also show the asymmetry in the Born approximation without taking any detector related effects into account (dotted line). The finite lepton rapidity coverage and the $|\cos\theta^*|$ cut significantly reduce the forward backward asymmetry in magnitude. Energy and momentum resolution effects broaden the Z peak and thus introduce a characteristic S type bending in A_{FB} at $m(\ell^+\ell^-) \approx M_Z$. Analogous to the di-lepton invariant mass distribution, lepton identification requirements substantially reduce the impact of QED radiative corrections on the forward backward asymmetry below the Z peak. For $m(\ell^+\ell^-) > 100$ GeV, they have only a small effect on A_{FB}, similar to the case where no detector effects are taken into account.

Although QED corrections to the forward backward asymmetry are reduced in magnitude for $m(\ell^+\ell^-) < M_Z$ by experimental lepton detection and identification requirements, they are still considerably larger than the NLO QCD corrections in this region. This is demonstrated in Fig. 10 for the electron final state. Similar results are obtained for $p\bar{p} \to \mu^+\mu^-(\gamma)$. The $\mathcal{O}(\alpha_s)$ QCD corrections to $p\bar{p} \to Z, \gamma^* \to \ell^+\ell^- X$ are calculated in the $\overline{\rm MS}$ scheme using the Monte Carlo approach of Ref. [19]. The calculation generalizes that of Ref. [42] to include finite Z width effects and virtual photon exchange diagrams. The QCD corrections to A_{FB} [43] are found to be quite small. Below (above) the Z peak, the magnitude of the forward backward asymmetry is reduced by typically $\delta A_{FB}/A_{FB} \approx -0.05$ ($\delta A_{FB}/A_{FB} \approx -0.02$). For 75 GeV $< m(\ell^+\ell^-) <$ 105 GeV, NLO QCD corrections decrease the integrated asymmetry by $\delta A_{FB}/A_{FB} \approx -0.03$. QED and QCD corrections to the integrated forward backward asymmetry in the Z peak region have opposite signs.

To reduce the background from heavy flavor production processes, the leptons in Z boson events are often required to be isolated. A lepton isolation cut typically requires the transverse energy in a cone of size R_0 about the direction of the lepton, $E_T^{R_0}$, to be less than a fraction, ϵ_E, of the lepton transverse energy $E_T(\ell)$, *i.e.*

$$\frac{E_T^{R_0} - E_T(\ell)}{E_T(\ell)} < \epsilon_E. \tag{23}$$

Sometimes the energy, E, instead of the transverse energy is used in the isolation requirement, Eq. (23). The isolation requirement and the cut imposed on the photon energy in the muon case have similar effects. In Fig. 11, we show how the lepton isolation requirement of Eq. (23) with $R_0 = 0.4$ and $\epsilon_E = 0.1$ modifies the effect of the $\mathcal{O}(\alpha)$ QED corrections on the di-lepton invariant mass distribution in the Z peak region. The isolation cut is seen to mostly affect the mass region below M_Z, reducing the maximum enhancement of the differential cross section by QED radiative corrections from a factor ~ 1.6 to $1.2 - 1.3$. In our calculation, for electrons, the isolation requirement is only imposed if the electron and photon are not recombined. $\mathcal{O}(\alpha\alpha_s)$ corrections to di-lepton production are not included in the results presented. These corrections are expected to increase $E_T^{R_0}$ somewhat, and therefore will modify the effect of the isolation cut.

In the past, the measurement of the W and Z boson cross sections has provided a test of perturbative QCD [44–46]. With the large data set accumulated in the 1994-95 Tevatron collider run, the uncertainty associated with the integrated luminosity ($\approx 3.6\%$ [46]) becomes a limiting factor in this measurement. This suggests to use the measured W and Z boson cross sections to determine the integrated luminosity in future experiments [46,47]. In order to accurately measure the integrated luminosity, it will be necessary not only to take the $\mathcal{O}(\alpha_s^2)$ corrections to the W and Z boson cross sections into account, but also to correct for higher order QED effects.

Experimentally, the Z boson cross section is extracted from the di-lepton cross section in a specified invariant mass interval around the Z boson mass, correcting for photon exchange and γZ interference effects. The size of the $\mathcal{O}(\alpha)$ QED corrections to the total di-lepton cross section is sensitive to the lepton identification criteria, the acceptance cuts and the range of the di-lepton invariant masses selected (see Fig. 11). In Table II we list the cross section ratio ("QED K-factor")

$$K^{QED} = \frac{\sigma^{\mathcal{O}(\alpha^3)}}{\sigma^{\rm Born}} \tag{24}$$

for 75 GeV $< m(\ell^+\ell^-) <$ 105 GeV ($\ell = e, \mu$). For comparison, we also tabulate the corresponding QCD K-factor,

$$K^{QCD} = \frac{\sigma^{\mathcal{O}(\alpha_s)}}{\sigma^{\rm Born}} \ . \tag{25}$$

One observes that the effect of the large QED corrections found in $d\sigma/dm(\ell^+\ell^-)$ is strongly reduced when integrating over a range in invariant mass which is approximately centered at M_Z. Nevertheless, the QED corrections usually are not negligible when compared with the $\mathcal{O}(\alpha_s)$ QCD corrections. QCD corrections enhance the Z boson production rate, whereas QED effects decrease the cross section for the invariant mass window chosen here. The total $p\bar{p} \to e^+e^-X$ ($p\bar{p} \to \mu^+\mu^-X$) cross section is reduced by about 7% (3%) by QED radiative corrections. As we have noted before, the dominant QED correction terms are proportional to $\log(\hat{s}/m_\ell^2)$ in absence of detector related effects. Without detector effects taken into account, QED corrections to $p\bar{p} \to e^+e^-X$ thus are larger than for di-muon production. The recombination of electron and photon momenta when the opening angle between the two particles is small strongly reduces the effect of the QED corrections to the integrated e^+e^- cross section. In the muon case, lepton identification requirements increase the magnitude of the QED corrections, and they almost compensate the cross section enhancement originating from $\mathcal{O}(\alpha_s)$ QCD corrections. Requiring the lepton to be isolated reduces the hard photon contribution to the $\mathcal{O}(\alpha^3)$ cross section, and hence increases the effect of the QED corrections. QCD corrections are only slightly modified by detector effects.

Since the $\mathcal{O}(\alpha)$ QED corrections and the $\mathcal{O}(\alpha_s)$ QCD corrections are of similar magnitude in the muon case when realistic experimental conditions are taken into account, one expects that the $\mathcal{O}(\alpha\alpha_s)$ and $\mathcal{O}(\alpha_s^2)$ corrections are also of similar size in this channel. The $\mathcal{O}(\alpha\alpha_s)$ corrections may thus be non-negligible in a precise determination of the integrated luminosity from the $Z \to \mu^+\mu^-$ cross section.

Finite detector acceptance cuts do not significantly modify the QED corrections to $d\sigma/dm(\ell^+\ell^-)$ and A_{FB}, except in the threshold region, $m(\ell^+\ell^-) \approx 2p_T^{cut}(\ell)$. The effect

of the cuts can be more pronounced in other distributions. As an example, we show the ratio of the lepton transverse momentum distribution at $\mathcal{O}(\alpha^3)$ and in the Born approximation in Fig. 12. All criteria which are necessary to simulate lepton detection and identification, except the isolation cut of Eq. (23), are imposed in this figure. For the CDF inspired pseudorapidity and p_T cuts we use in the muon case, the $2 \to 2$ phase space becomes much more restricted than the $2 \to 3$ phase space close to the p_T threshold. As a result, the cross section ratio exhibits a bump located at $p_T(\mu) \approx 30$ GeV (dashed line). Replacing the acceptance cuts by those used for electrons, the bump in the cross section disappears (dotted line). For $p_T(\mu) > 40$ GeV, the size of the radiative corrections is almost independent of the pseudorapidity and transverse momentum cuts imposed. Radiative corrections smear out the Jacobian peak, causing a characteristic dip in the cross section ratio at $p_T(\mu) \approx M_Z/2$. However, in this region, the cross section is subject to large QCD corrections [48] which are not taken into account in our calculation.

The QED corrections to the muon transverse momentum distribution reduce the cross section by 10 – 15% over most of the p_T range. For comparison, we also display the ratio of differential cross sections for $p\bar{p} \to e^+e^-(\gamma)$ in Fig. 12. Here, the $\mathcal{O}(\alpha)$ QED corrections are of $\mathcal{O}(1\%)$, except for the Jacobian peak region, $p_T(e) \approx 45$ GeV, where they reduce the cross section by up to 7%. The pronounced difference in radiative corrections between electrons and muons is largely due to the different lepton identification requirements discussed earlier in this subsection.

C. Radiative Corrections and the Z Boson Mass

As we have seen, final state bremsstrahlung severely distorts the Breit-Wigner shape of the Z resonance curve. As a result, QED corrections must be included when the Z boson mass is extracted from data, otherwise the mass extracted is shifted to a lower value. In absence of detector effects, the Z mass shift is approximately given by [36]

$$\Delta M_Z \approx -\frac{\pi\beta}{8} \ , \ z, \tag{26}$$

with β defined in Eq. (12). For $Z \to e^+e^-$ ($Z \to \mu^+\mu^-$), $\Delta M_Z \approx -110$ MeV ($\Delta M_Z \approx -60$ MeV). However, as it is clear from the previous section, detector effects significantly modify ΔM_Z.

The Z boson mass extracted from Tevatron experiments serves as a reference point when compared with the precise measurement performed at LEP. It helps to calibrate the electromagnetic energy scale, and to determine the electron energy resolution as well as the muon momentum resolution which are important for the measurement of the W mass.

In the approximate treatment of the QED corrections used so far by the Tevatron experiments, only final state corrections are taken into account. In addition, the effects of soft and virtual corrections are estimated from the inclusive $\mathcal{O}(\alpha^2)$ $Z \to \ell^+\ell^-(\gamma)$ width [49] and the hard photon bremsstrahlung contribution [13].

We now study the differences in the Z boson masses extracted using the approximation currently employed in the experimental analysis and our complete $\mathcal{O}(\alpha^3)$ QED calculation, and investigate the effect of the initial state radiative corrections on the Z mass shift. To extract the Z boson mass, we use a log-likelihood fit to the shape of the di-lepton invariant mass distribution in the range 81 GeV$< m(\ell^+\ell^-) <$ 101 GeV. The templates for the $m(\ell^+\ell^-)$ distributions are calculated using the lowest order differential cross section, varying M_Z between 90.6 GeV and 91.5 GeV in steps of 100 MeV. Detector effects are simulated as described in Sec. IIIB. No isolation cut [Eq. (23)] is imposed on the charged leptons. The soft and collinear cutoff parameters are chosen to be $\delta_s = 10^{-3}$ and $\delta_c = 3 \times 10^{-4}$. In order to be able to determine ΔM_Z, it is necessary to properly include the radiation of photons with an energy which is of the same order as the shift in M_Z, using the full $2 \to 3$ phase space. δ_s and δ_c, therefore, have to be smaller than about 2×10^{-3}, otherwise a non-negligible dependence of the Z boson mass shift, ΔM_Z, on these parameters remains.

The error on the Z mass resulting from the statistical uncertainties in the Monte Carlo event samples and the finite step size in varying M_Z in the templates is approximately 5 MeV in our simulation. This is adequate for the semi-quantitative analysis reported here. It is straightforward to reduce the uncertainty by increasing the number of events generated and

the number of templates used, given sufficient computing power.

For definiteness, we concentrate on the electron channel. Results similar to those which we obtain are expected in the muon case. The shift in M_Z induced by the QED corrections is determined by comparing the shape of the $\mathcal{O}(\alpha^3)$ e^+e^- invariant mass distribution for the nominal value of $M_Z = 91.187$ GeV with that of the templates, and calculating the log-likelihood as a function of the Z boson mass used as input in the templates. Repeating this procedure 1000 times with 10,000 events each, the difference between the average of the mass which maximizes the log-likelihood and the nominal Z boson mass is then identified with the shift induced by the QED corrections. The same procedure is carried out to compute the Z mass shift if the approximate calculation of Ref. [13] is used. The Z boson mass obtained from the complete $\mathcal{O}(\alpha^3)$ cross section is found to be about 10 MeV smaller than that obtained using the approximate calculation. Most of the change can be attributed to the different treatment of the final state soft and virtual corrections in the two calculations. A change of 10 MeV in M_Z translates into a shift of several MeV in M_W through the dependence of the energy scale and the momentum resolution on the Z boson mass measured [8,9]. For the current level of precision, this small shift is unimportant. However, it cannot be ignored for a high-precision measurement of M_W.

In order to estimate how initial state corrections and initial – final state interference correction terms affect the Z boson mass, we compare the mass obtained using the full $\mathcal{O}(\alpha)$ corrections with that extracted when final state radiative corrections are taken into account only. The two values of M_Z are found to agree within the numerical accuracy of our simulation. Initial state radiative corrections and initial – final state interference correction terms therefore contribute very little to the Z boson mass shift. As we have discussed in Sec. II, current fits to the PDF's do not include QED effects. This introduces theoretical uncertainties, such as a strong dependence of the initial state corrections on the factorization scheme used. However, since initial state corrections essentially do not contribute to the Z boson mass shift, these uncertainties will have no significant effect on the Z boson mass extracted. This conjecture is supported by the fact that the numerical values for the mass

shifts in the QED $\overline{\rm MS}$ and DIS scheme are the same.

The Z boson mass extracted from the fit to the di-lepton invariant mass distribution also depends on the PDF uncertainties, and the choice of the renormalization and factorization scale. At present, PDF's which take into account uncertainties in their fit are not generally available[2]. We therefore only consider the scale dependence here. Changing $Q^2 = \mu^2 = M^2_{QED} = M^2_{QCD}$ from $Q^2 = \hat{s}$ to $Q^2 = 100\,\hat{s}$ decreases the fitted Z mass by 10 MeV both in the Born approximation and when $\mathcal{O}(\alpha)$ corrections are taken into account. This indicates that the Z boson mass shift caused by QED corrections is insensitive to the choice of Q^2. The scale dependence of the fitted Z mass is eliminated when $\mathcal{O}(\alpha_s)$ QCD corrections are taken into account.

IV. THE FORWARD BACKWARD ASYMMETRY AT THE LHC

As we have mentioned in the Introduction, one can use $\sin^2\theta^{lept}_{eff}$ together with m_{top} to constrain the Higgs boson mass. At LEP, $\sin^2\theta^{lept}_{eff}$ has been measured with an accuracy of approximately ± 0.00024 [1]. In order to extract the Higgs boson mass with a precision of $\delta M_H/M_H \approx 30\%$ or better, the uncertainty in $\sin^2\theta^{lept}_{eff}$ has to be reduced by at least a factor two. At the LHC (pp collisions at $\sqrt{s} = 14$ TeV), the $Z \to \ell^+\ell^-$ cross section is approximately 1.6 nb for each lepton flavor. For the projected yearly integrated luminosity of 100 fb^{-1}, this results in a very large number of $Z \to \ell^+\ell^-$ events which, in principle, can be used to measure the forward backward asymmetry and thus $\sin^2\theta^{lept}_{eff}$ with extremely high precision [11]. In this Section, we investigate the prospects to measure $\sin^2\theta^{lept}_{eff}$ using the forward backward asymmetry at the LHC, taking into account the $\mathcal{O}(\alpha)$ QED and $\mathcal{O}(\alpha_s)$ QCD corrections. At LHC luminosities, it is easier to trigger on $\mu^+\mu^-$ than on e^+e^- pairs in the Z mass region [51,52]. In our analysis, we therefore concentrate on the $Z \to \mu^+\mu^-$ channel; qualitatively similar results are obtained for the electron channel.

---

[2] An approach to extract PDF's including systematic errors has recently been described in Ref. [50].

In pp collisions, the quark direction in the initial state has to be extracted from the boost direction of the di-lepton system with respect to the beam axis [53]. The cosine of the angle between the lepton and the quark in the $\ell^+\ell^-$ rest frame is then approximated by

$$\cos\theta^* = \frac{|p_z(\ell^+\ell^-)|}{p_z(\ell^+\ell^-)} \; \frac{2}{m(\ell^+\ell^-)\sqrt{m^2(\ell^+\ell^-)+p_T^2(\ell^+\ell^-)}} \left[p^+(\ell^-)p^-(\ell^+) - p^-(\ell^-)p^+(\ell^+)\right]. \quad (27)$$

For the definition of $\cos\theta^*$ given in Eq. (15), $A_{FB} = 0$ for pp collisions.

At the LHC, the sea – sea quark flux is much larger than at the Tevatron. As a result, the probability, f_q, that the quark direction and the boost direction of the di-lepton system coincide is significantly smaller than one. The forward backward asymmetry is therefore smaller than at the Tevatron. Events with a large rapidity of the di-lepton system, $y(\ell^+\ell^-)$, originate from collisions where at least one of the partons carries a large fraction x of the proton momentum. Since valence quarks dominate at high values of x, a cut on the di-lepton rapidity increases f_q, and thus the asymmetry [53] and the sensitivity to the effective weak mixing angle.

The forward backward asymmetry at the LHC, using Eq. (27) to define $\cos\theta^*$, and imposing a

$$|y(\mu^+\mu^-)| > 1 \quad (28)$$

cut, is shown in Fig. 13 for values of $m(\mu^+\mu^-)$ up to 250 GeV. No other cuts besides the $y(\mu^+\mu^-)$ cut have been imposed in Fig. 13. Without the cut of Eq. (28), A_{FB} would be approximately a factor 1.25 smaller. Although the di-lepton rapidity cut enhances the asymmetry, it is about a factor 1.5 smaller than at the Tevatron.

Qualitatively, the behaviour of the forward backward asymmetry as a function of the di-lepton invariant mass is similar to that in $p\bar{p}$ collisions. Furthermore, QED and QCD corrections are seen to have a quantitatively similar effect on A_{FB} as in $p\bar{p}$ collisions. In the Z peak region, 75 GeV $< m(\mu^+\mu^-) <$ 105 GeV, the integrated forward backward asymmetry can again be parameterized by Eqs. (17) and (19) with

$$a^{\rm Born} = 0.2458, \qquad b^{\rm Born} = 2.19, \quad (29)$$

$$\Delta a^{\rm QED} = 0.0008, \qquad \Delta b^{\rm QED} = -0.09. \tag{30}$$

and

$$\Delta a^{\rm QCD} = -0.0011, \qquad \Delta b^{\rm QCD} = 0.06. \tag{31}$$

From Eqs. (29) and (18) we observe that the parameter a is essentially the same as at Tevatron energies. b, on the other hand, which controls the sensitivity to the weak mixing angle, is significantly reduced. QED corrections increase the integrated asymmetry in the peak region by about $\delta A_{FB}/A_{FB} \approx 0.02$, and slightly reduce the sensitivity to $\sin^2\theta_{eff}^{lept}$. QCD corrections are found to reduce it by approximately $\delta A_{FB}/A_{FB} \approx -0.05$. QED and QCD corrections to the integrated forward backward asymmetry in the Z peak region have opposite sign, as at the Tevatron.

Using Eqs. (29) and (31) together with Eqs. (13) and (14), it is now straightforward to estimate the error expected for $\sin^2\theta_{eff}^{lept}$ from a measurement of the forward backward asymmetry in the Z peak region at the LHC. For an integrated luminosity of 100 fb^{-1}, we find that it should be possible to measure $\sin^2\theta_{eff}^{lept}$ with a statistical precision of

$$\delta \sin^2\theta_{eff}^{lept} = 3.9 \times 10^{-5}. \tag{32}$$

Both, NLO QCD and QED corrections have been taken into account in this estimate. The $|y(\mu^+\mu^-)| > 1$ cut improves the precision for $\sin^2\theta_{eff}^{lept}$ by about 10%. Our result is about 35% better than the estimate given in Ref. [11]. The shift in A_{FB} introduced by the combined QED and QCD radiative corrections is about a factor 7 larger than the expected statistical error.

The estimate of Eq. (32) has been obtained assuming full rapidity coverage for the muons. The proposed FELIX experiment [54] is expected to achieve this. However, FELIX will operate at a reduced luminosity of at most $\mathcal{L} = 10^{33}$ cm^{-2}s^{-1}, corresponding to a yearly integrated luminosity of 10 fb^{-1} at best. For 10 fb^{-1} the expected precision is $\delta \sin^2\theta_{eff}^{lept} \approx 1.2 \times 10^{-4}$. In both the ATLAS and CMS detector, muons can only be detected for pseudo-rapidities $|\eta(\mu)| < 2.4$ [51,52]. In Fig. 14 we display the forward backward asymmetry at the

LHC imposing a $|\eta(\mu)| < 2.4$ cut in addition to the di-lepton rapidity cut of Eq. (28). The finite rapidity range covered by the detector is seen to dramatically reduce the asymmetry. In the region around the Z pole, the integrated forward backward asymmetry is again an approximately linear function of $\sin^2\theta_{eff}^{lept}$ (see Eq. (17)) with

$$a^{\rm Born} = 0.2464, \qquad\qquad b^{\rm Born} = 0.72. \tag{33}$$

QED and QCD radiative corrections shift these values by

$$\Delta a^{\rm QED} = 0.0024, \qquad\qquad \Delta b^{\rm QED} = -0.07, \tag{34}$$

and

$$\Delta a^{\rm QCD} = 0.0067, \qquad\qquad \Delta b^{\rm QED} = -0.27, \tag{35}$$

respectively. The parameter b, which directly controls the sensitivity to $\sin^2\theta_{eff}^{lept}$, is reduced by about a factor 3 by the finite rapidity acceptance. QED corrections further reduce b by approximately 10%, and QCD corrections by an additional 30%. The finite rapidity coverage also results in a reduction of the total Z boson cross section by roughly a factor 5. As a result, the uncertainty expected for $\sin^2\theta_{eff}^{lept}$ with 100 fb^{-1} increases by more than a factor 10 to

$$\delta\sin^2\theta_{eff}^{lept} = 4.4\times10^{-4} \qquad \text{for} \qquad |\eta(\mu)| < 2.4. \tag{36}$$

The shift in A_{FB} introduced by the combined QCD and QED radiative corrections is about a factor 1.5 larger than the statistical error expected.

The rapidity range covered by the electromagnetic calorimeter and the tracking system is very similar to that of the muon system [51,52]. For e^+e^- production, one therefore does not expect to measure $\sin^2\theta_{eff}^{lept}$ with a higher precision than in the muon channel. As in the Tevatron case discussed in Sec. IIIA, the QED corrections to A_{FB} in absence of detector effects are more pronounced in the electron case. A $p_T(\ell) > 20$ GeV cut has essentially no effect on the forward backward asymmetry in the Z peak region.

The precision expected for $\sin^2\theta^{lept}_{eff}$ from LHC experiments should be compared with the accuracy from current LEP and SLC data [1], and with the sensitivity expected from future experiments at the SLC and the Tevatron. The combined uncertainty of $\sin^2\theta^{lept}_{eff}$ from LEP and SLC experiments is approximately 2.4×10^{-4}. With the planned luminosity upgrade [55], one hopes to collect 3×10^6 Z boson events at the SLC. This would allow to measure $\sin^2\theta^{lept}_{eff}$ from the left right asymmetry with a precision of about 1.2×10^{-4}, which is similar to the one attainable by FELIX with 10 fb^{-1}. At the Tevatron, with the same integrated luminosity, one expects an uncertainty of 2.3×10^{-4} for $\sin^2\theta^{lept}_{eff}$ [4] per experiment. In order to improve the precision beyond that expected from future SLC and Tevatron experiments, it will be necessary to detect leptons in the very forward pseudorapidity range, $|\eta| = 3.0 - 5.0$ at the LHC when it operates at the design luminosity of $\mathcal{L} = 10^{34}$ cm^{-2}s^{-1}.

V. SUMMARY AND CONCLUSIONS

In a precision measurement of M_W in hadronic collisions, a simultaneous determination of M_Z in di-lepton production is required for calibration purposes. The forward backward asymmetry makes it possible to determine $\sin^2\theta^{lept}_{eff}$ with high precision. Both measurements help to constrain the Higgs boson mass from radiative corrections. In order to perform these high precision measurements, it is crucial to fully control higher order QCD and electroweak corrections. In this paper we have presented a calculation of di-lepton production in hadronic collisions based on a combination of analytic and Monte Carlo integration techniques which includes initial and final state $\mathcal{O}(\alpha)$ QED corrections. Previous calculations [13,14] have been based on the final state photonic corrections, estimating the virtual corrections indirectly from the inclusive $\mathcal{O}(\alpha^2)$ $Z \to \ell^+\ell^-(\gamma)$ width and the hard photon bremsstrahlung contribution.

Due to mass singular logarithmic terms associated with final state photon radiation in the limit where the photon is collinear with one of the leptons, final state radiation effects dominate. Initial state corrections were found to be small after factorizing the corresponding

collinear singularities into the parton distribution functions. QED corrections to the evolution of the parton distribution functions and purely weak corrections are not included in our calculation; they are expected to be small. Initial state QED corrections are uniform over the entire di-lepton invariant mass range. In contrast, final state corrections vary rapidly with $m(\ell^+\ell^-)$, and strongly modify the shape of the invariant mass distribution as a large fraction of the events shifts from the Z boson peak to lower invariant masses (see Figs. 3 and 4). Below M_Z, radiative corrections enhance the cross section by up to a factor 2.7 (1.9) for electrons (muons).

QED corrections also strongly reduce the magnitude of the forward backward asymmetry, A_{FB}, for di-lepton invariant masses between 50 GeV and 90 GeV. In the Z peak region, 75 GeV $< m(\ell^+\ell^-) <$ 105 GeV, they enhance the integrated forward backward asymmetry by up to 8%.

When detector effects are taken into account, the effect of the mass singular logarithmic terms in the electron case is strongly reduced. The granularity of the detector and the size of the electromagnetic showers in the calorimeter make it difficult to discriminate between electrons and photons with a small opening angle. One therefore combines the electron and photon four momentum vectors if both particles traverse the same calorimeter cell. In the muon case, the energy of the photon is required to be smaller than a critical value, E_c^γ, if both particles traverse the same calorimeter cell, and mass singular terms survive. Removing energetic photons reduces (enhances) the effect of the $\mathcal{O}(\alpha)$ corrections below (above) M_Z. Detector effects are also found to considerably decrease the size of the QED corrections to the forward backward asymmetry below the Z peak for $p\bar{p} \to \mu^+\mu^-(\gamma)$.

QED corrections have a significant impact on the di-lepton cross section in the Z peak region, and the Z mass extracted from experiment. In future Tevatron runs, the total W/Z cross section may be used as a luminosity monitor [46]. As shown in Table II, QED corrections can reduce the di-lepton cross section in the Z peak region by up to 10%. Final state radiative corrections are known [8,9] to substantially shift the Z boson mass. The Z boson mass extracted from our $\mathcal{O}(\alpha^3)$ $\ell^+\ell^-$ invariant mass distribution was found to be

about 10 MeV smaller than that obtained using the approximate calculation of Ref. [13]. Initial state corrections and initial – final state interference terms only marginally influence the amount the Z boson mass is shifted. The contribution of the QED corrections to the PDF's is expected to be of the size of the initial state radiative corrections that are included in our calculation. It is unlikely to be a limiting factor in the determination of the Z (and W) boson mass in hadronic collisions.

For the current level of precision, the approximate calculation of Ref. [13] appears to be adequate. The small difference in the Z boson mass obtained in the complete $\mathcal{O}(\alpha^3)$ and the approximate calculation, however, cannot be ignored if one attempts to measure the W mass with high precision at hadron colliders. This also raises the question of how strongly multiple final state photon radiation influences the measured Z boson mass. Using the fragmentation function approach, we have shown that higher order QED corrections non-trivially modify the shape of the di-lepton invariant mass distribution. They may introduce an additional shift of M_Z by $\mathcal{O}(10$ MeV), and may have a non-negligible impact on the forward backward asymmetry. So far, only partial calculations exist [56]. A more complete understanding of multiple photon radiation is warranted.

Finally, we studied the forward backward asymmetry at the LHC. The very large number of Z bosons produced at the LHC offers an opportunity to accurately measure $\sin^2\theta^{lept}_{eff}$ from A_{FB}. For the forward backward asymmetry to be non-zero in pp collisions, the scattering angle has to be defined with respect to the boost direction of the lepton pair along the beam axis. Imposing a $|y(\ell^+\ell^-)| > 1$ cut reduces the fraction of events where the quark direction is misidentified. It enhances the asymmetry by a factor 1.25, and thus improves the sensitivity to $\sin^2\theta^{lept}_{eff}$ by about 10%. With a detector possessing full rapidity coverage for leptons, $\sin^2\theta^{lept}_{eff}$ can in principle be measured with a precision of $\delta\sin^2\theta^{lept}_{eff} = 3.9\times10^{-5}$ if an integrated luminosity of 100 fb^{-1} is achieved. The shift in A_{FB} introduced by QED and QCD radiative corrections is about one order of magnitude larger than the statistical error expected. The finite lepton rapidity coverage of the ATLAS and CMS detectors strongly reduces A_{FB} and the number of Z bosons produced, which results in an increase of the

uncertainty in $\sin^2\theta_{eff}^{lept}$ by about a factor 10. In order to significantly improve the precision for $\sin^2\theta_{eff}^{lept}$ beyond that expected from future SLC and Tevatron experiments, it will thus be necessary to detect electrons and muons in the very forward pseudorapidity range, $|\eta| = 3.0 - 5.0$, at the LHC, and to achieve an integrated luminosity of $\mathcal{O}(100\ \text{fb}^{-1})$.

ACKNOWLEDGMENTS

We would like to thank I. Adam, A. Bodek, M. Demarteau, S. Errede, E. Flattum, H. Frisch, F. Halzen, Y.K. Kim, E. Laenen, M. Strikman, C. Taylor, and D. Wackeroth for useful and stimulating discussions. One of us (U.B.) is grateful to the Fermilab Theory Group, where part of this work was carried out, for its generous hospitality. This work has been supported in part by Department of Energy contract No. DE-AC02-76CHO3000 and NSF grant PHY-9600770.

REFERENCES

[1] M. Demarteau, FERMILAB-Conf/96-354, to appear in the Proceedings of the *"DPF96 Conference"*, Minneapolis, MN, August 10 – 15, 1996; D. Abbaneo *et al.* (LEP Electroweak Working Group), CERN-PPE/96-183 (preprint, December 1996).

[2] M. Lancaster, FERMILAB-Conf-97/176-E, to appear in the proceedings of the *"Le Recontres de Physique de la Vallée d' Aoste"*, La Thuile, Italy, March 3 – 7, 1997.

[3] T. Rizzo, Mod. Phys. Lett. **A6**, 1961 (1991); J. Ellis, G. Fogli and E. Lisi, Phys. Lett. **B274**, 456 (1992) and Phys. Lett. **B318**, 148 (1993).

[4] H. Aihara *et al.*, in *"Future Electroweak Physics at the Fermilab Tevatron: Report of the TEV_2000 Study Group"*, eds. D. Amidei and R. Brock, FERMILAB-Pub/96-082, p. 63 (April 1996); U. Baur and M. Demarteau, FERMILAB-Conf/96-423, to appear in the Proceedings of the Workshop *"New Directions in High Energy Physics"*, Snowmass, CO, June 25 – July 12, 1996; K. Hagiwara, D. Haidt and S. Matsumoto, KEK-TH-512, DESY 96-192, (preprint), to appear in Z. Phys. **C**.

[5] A. Ballestrero *et al.*, in *"Physics at LEP2"*, eds. G. Altarelli, T. Sjostrand and F. Zwirner, CERN Yellow Report, CERN-96-01, Vol. 1, p. 141.

[6] J.P. Marriner, FERMILAB-Conf-96/391, to appear in the Proceedings of the Workshop *"New Directions in High Energy Physics"*, Snowmass, CO, June 25 – July 12, 1996; P.P. Bagley *et al.*, FERMILAB-Conf-96/392, to appear in the Proceedings of the Workshop *"New Directions in High Energy Physics"*, Snowmass, CO, June 25 – July 12, 1996; D.A. Finley, J. Marriner and N.V. Mokhov, FERMILAB-Conf-96/408, presented at the *"Conference on Charged Particle Accelerators"*, Protvino, Russia, October 22 – 24, 1996.

[7] S. Keller and J. Womersley, FERMILAB-Conf-96/422-T, to appear in the Proceedings of the Workshop *"New Directions in High Energy Physics"*, Snowmass, CO, June 25 –

July 12, 1996.

[8] F. Abe *et al.* (CDF Collaboration), Phys. Rev. Lett. **75**, 11 (1995) and Phys. Rev. **D52**, 4784 (1995).

[9] S. Abachi *et al.* (DØ Collaboration), Phys. Rev. Lett. **77**, 3309 (1996), and FERMILAB-Conf/96-251-E, submitted to the *"28$^{\rm th}$ International Conference on High Energy Physics"*, Warsaw, Poland, 25 – 31 July 1996.

[10] D. Bardin *et al.*, CERN-TH. 6443/92 (preprint); P. Gambino and A. Sirlin, Phys. Rev. **D49**, 1160 (1994).

[11] P. Fisher, U. Becker and P. Kirkby, Phys. Lett. **B356**, 404 (1995).

[12] C. Albajar *et al.* (UA1 Collaboration), Z. Phys. **C44**, 15 (1989); F. Abe *et al.* (CDF Collaboration), Phys. Rev. Lett. **67**, 1502 (1991); P. Hurst (CDF Collaboration), Ph.D. Thesis, University of Illinois at Urbana – Champaign, 1990.

[13] F. Berends and R.K. Kleiss, Z. Phys. **C27**, 365 (1985).

[14] R.G. Wagner, Comput. Phys. Commun. **70**, 15 (1992).

[15] F. Abe *et al.* (CDF Collaboration), Phys. Rev. **D49**, R1 (1994).

[16] J. Rosner, Phys. Lett. **B221**, 85 (1989), and Phys. Rev. **D54**, 1078 (1996).

[17] F. Abe *et al.* (CDF Collaboration), Phys. Rev. **D51**, 949 (1995).

[18] F. Abe *et al.* (CDF Collaboration), Phys. Rev. Lett. **77**, 2616 (1996).

[19] H. Baer, J. Ohnemus, and J.F. Owens, Phys. Rev. **D40**, 2844 (1989) and Phys. Rev. **D42**, 61 (1990); L. Bergmann, Ph.D. dissertation, Florida State University, report No. FSU-HEP-890215, 1989 (unpublished); W. Giele and E.W.N. Glover, Phys. Rev. **D46**, 1980 (1992).

[20] U. Baur and E.L. Berger, Phys. Rev. **D47**, 4889 (1993).

[21] U. Baur and D. Zeppenfeld, Phys. Rev. Lett. **75**, 1002 (1995).

[22] J. Kripfganz and H. Perlt, Z. Phys. **C41**, 319 (1988); H. Spiesberger, Phys. Rev. **D52**, 4936 (1995).

[23] A. de Rujula, R. Petronzio and A. Savoy-Navarro, Nucl. Phys. **B154**, 394 (1979).

[24] D.B. DeLaney *et al.*, Phys. Rev. **D47**, 853 (1993); Phys. Lett. **B292**, 413 (1992), (E) Phys. Lett. **B302**, 540 (1993); G. Siopsis *et al.*, Acta Phys. Polon. **B23**, 1133 (1992).

[25] D. Bousard *et al.* (The LHC Study Group), CERN/AC/95-05 (October 1995).

[26] G.'t Hooft and M. Veltman, Nucl. Phys. **B44**, 189 (1972).

[27] V.N. Gribov and L.N. Lipatov, Sov. J. Nucl. Phys. **15**, 78 (1972); Yu.L. Dokshitzer, JETP **73**, 1216 (1977); G. Altarelli and G. Parisi, Nucl. Phys. **B126**, 298 (1977).

[28] A. Martin, R.G. Roberts, and W.J. Stirling, Phys. Lett. **B354**, 155 (1995) and Phys. Lett. **B387**, 419 (1996); H. Lai *et al.* (CTEQ Collaboration), Phys. Rev. **D51**, 4763 (1995) and Phys. Rev. **D55**, 1280 (1997).

[29] W.A. Bardeen, A.J. Buras, D.W. Duke, and T. Muta, Phys. Rev. **D18**, 3998 (1978).

[30] J. F. Owens and W. K. Tung, Annu. Rev. Nucl. Part. Sci. **42**, 291 (1992).

[31] H. Baer and M.H. Reno, Phys. Rev. **D43**, 2892 (1991).

[32] M. Böhm and W. Hollik, Nucl. Phys. **B204**, 45 (1982).

[33] W. Hollik, Fort. Phys. **38**, 165 (1990).

[34] A.D. Martin, R.G. Roberts, and W.J. Stirling, Phys. Rev. **D50**, 6734 (1994).

[35] T. Kinoshita, J. Math. Phys. **3**, 650 (1962); T.D. Lee and M. Nauenberg, Phys. Rev. **133**, B1549 (1964).

[36] F. Berends, in *"Physics at LEP 1"*, eds. G. Altarelli, R. Kleiss and C. Verzegnassi,

CERN 89-08, Vol. 1, p. 89.

[37] O. Nicrosini and L. Trentadue, Z. Phys. **C39**, 479 (1988).

[38] D. Bardin *et al.*, Nucl. Phys. **B351**, 1 (1991).

[39] J. Collins and D. Soper, Phys. Rev. **D16**, 2219 (1977).

[40] M. Böhm and W. Hollik, Phys. Lett. **B139**, 213 (1984).

[41] F. Abe *et al.* (CDF Collaboration), Phys. Rev. **D45**, 3921 (1992).

[42] H. Baer and M.H. Reno, Phys. Rev. **D45**, 1503 (1992).

[43] D. Callaway, Phys. Lett. **B108**, 421 (1982).

[44] S. Abachi *et al.* (DØ Collaboration), Phys. Rev. Lett. **75**, 1456 (1995).

[45] F. Abe *et al.* (CDF Collaboration), Phys. Rev. **D44**, 29 (1991) and Phys. Rev. Lett. **69**, 28 (1992).

[46] F. Abe *et al.* (CDF Collaboration), Phys. Rev. Lett. **76**, 3070 (1996).

[47] M. Dittmar, F. Pauss and D. Zürcher, ETHZ-IPP PR-97-01 (preprint, May 1997), submitted to Phys. Rev. **D**.

[48] G. Altarelli, R.K. Ellis, M. Greco and G. Martinelli, Nucl. Phys. **B246**, 12 (1984); P. Arnold and R. Kauffman, Nucl. Phys. **B349**, 381 (1991); H. Contapanagos and G. Sterman, Nucl. Phys. **B400**, 211 (1993); L. Alvero and H. Contapanagos, Nucl. Phys. **B456**, 497 (1995); W. Giele and S. Keller, FERMILAB-Pub-96/332-T (preprint, April 1997).

[49] D. Albert, W.J. Marciano, D. Wyler, and Z. Parsa, Nucl. Phys. **B166**, 460 (1980).

[50] S. Alekhin, hep-ph/9611213 (preprint, November 1996).

[51] D. Gingrich *et al.* (ATLAS Collaboration), ATLAS Letter of Intent, CERN-LHCC-92-4

(October 1992); W. W. Armstrong *et al.* (ATLAS Collaboration), ATLAS Technical Design Report, CERN-LHCC-94-43 (December 1994).

[52] M. Della Negra *et al.* (CMS Collaboration), CMS Letter of Intent, CERN-LHCC-92-3 (October 1992); G. L. Bayatian *et al.* (CMS Collaboration), CMS Technical Design Report, CERN-LHCC-94-38 (December 1994).

[53] M. Dittmar, Phys. Rev. **D55**, 161 (1997).

[54] K. Eggert and C. Taylor, CERN-PPE/96-136 (preprint, October 1996), submitted to Nucl. Phys.

[55] M. Breidenbach *et al.*, SLAC-CN-409 (1996).

[56] U. Baur, T. Han, N. Kauer, R. Sobey and D. Zeppenfeld, Phys. Rev. **D56**, 140 (1997); E. Richter-Was, Z. Phys. **C64**, 227 (1994); S. Laporta and R. Odorico, Nucl. Phys. **B266**, 633 (1986) and Comp. Phys. Comm. **39**, 127 (1986); R. Odorico, Comp. Phys. Comm. **59**, 527 (1990).

TABLES

TABLE I. The integrated forward backward asymmetry, A_{FB}, in $p\bar{p} \to e^+e^-X$ at $\sqrt{s} = 1.8$ TeV for 75 GeV $< m(e^+e^-) <$ 105 GeV and $m(e^+e^-) >$ 105 GeV. Shown are the SM predictions with and without $\mathcal{O}(\alpha)$ QED corrections together with the experimental values of Ref. [18]. The uncertainties listed for the theoretical results represent the statistical error of the Monte Carlo integration.

	75 GeV $< m(e^+e^-) <$ 105 GeV	$m(e^+e^-) >$ 105 GeV
A_{FB}^{Born}	0.048 ± 0.001	0.523 ± 0.001
$A_{FB}^{\mathcal{O}(\alpha^3)}$	0.052 ± 0.001	0.528 ± 0.001
$A_{FB}^{exp.}$	0.070 ± 0.016	0.43 ± 0.10

TABLE II. The cross section ratios $K^{QED} = \sigma^{\mathcal{O}(\alpha^3)}/\sigma^{\rm Born}$ and $K^{QCD} = \sigma^{\mathcal{O}(\alpha_s)}/\sigma^{\rm Born}$ for $p\bar{p} \to \ell^+\ell^-X$ ($\ell = e, \mu$) at $\sqrt{s} = 1.8$ TeV with 75 GeV $< m(\ell^+\ell^-) <$ 105 GeV. Shown are the predictions for three cases: without taking any detector effects into account ("no detector effects"), with the detector effects described in the text and no lepton isolation cut ("with detector effects, no lepton isolation"), and finally adding lepton isolation [see Eq. (23)] ("with detector effects, with lepton isolation").

	no detector effects	with detector effects	
		no lepton isolation	with lepton isolation
K^{QED} $(p\bar{p} \to e^+e^-X)$	0.93	0.98	0.96
K^{QED} $(p\bar{p} \to \mu^+\mu^-X)$	0.97	0.92	0.90
K^{QCD} $(p\bar{p} \to \ell^+\ell^-X)$	1.17	1.16	1.14

FIGURES

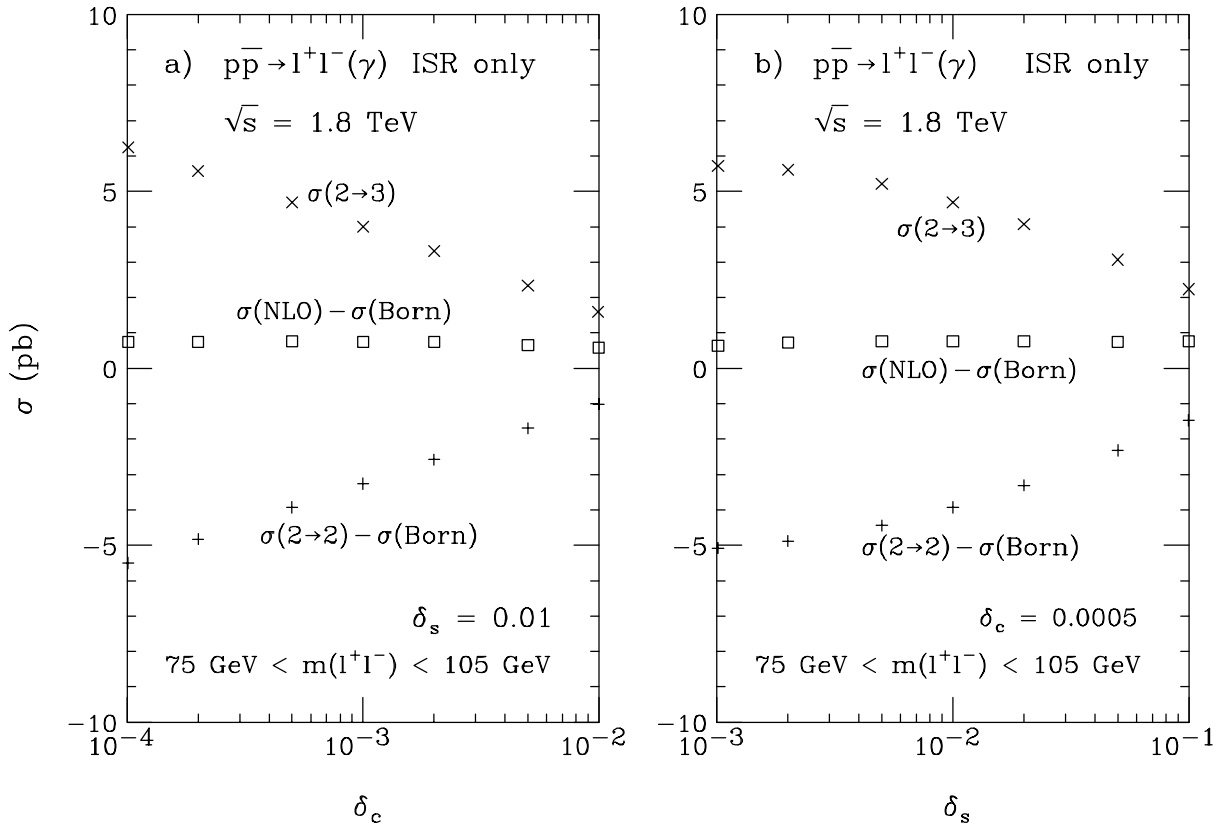

FIG. 1. The $p\bar{p} \to \ell^+\ell^-(\gamma)$, ($\ell = e, \mu$) cross section for $\sqrt{s} = 1.8$ TeV and 75 GeV $< m(\ell^+\ell^-)$ < 105 GeV as a function of a) δ_c for $\delta_s = 0.01$, and b) δ_s for $\delta_c = 0.0005$, including initial state radiation corrections only. Shown are $\sigma(2 \to 2) - \sigma(\mathrm{Born})$, $\sigma(2 \to 3)$, and $\sigma(\mathrm{NLO}) - \sigma(\mathrm{Born})$. $\sigma(\mathrm{NLO})$ denotes the $\mathcal{O}(\alpha^3)$ cross section.

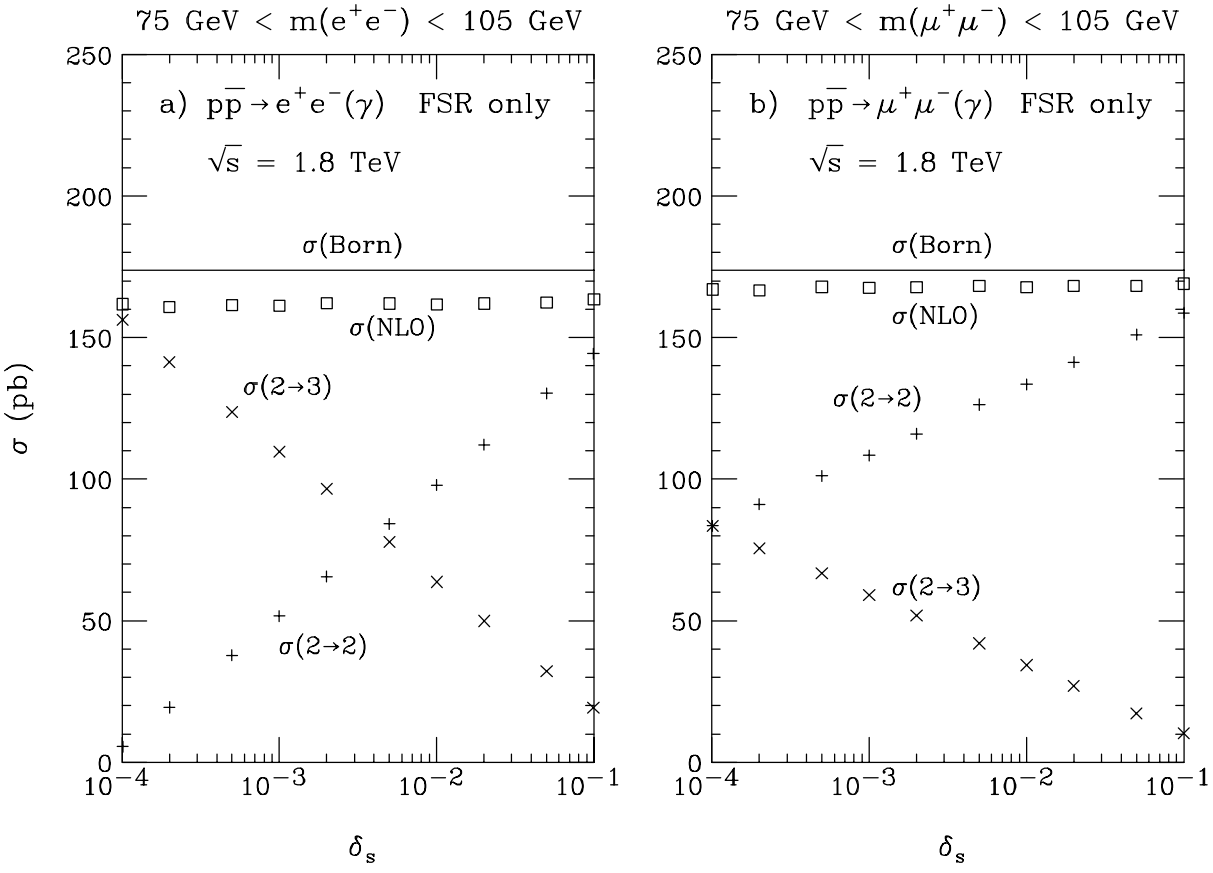

FIG. 2. The cross section a) $\sigma(p\bar{p} \to e^+e^-(\gamma))$ and b) $\sigma(p\bar{p} \to \mu^+\mu^-(\gamma))$ as a function of δ_s, including final state radiation corrections only, for $\sqrt{s} = 1.8$ TeV and 75 GeV $< m(\ell^+\ell^-) <$ 105 GeV. Shown are the $2 \to 2$ and $2 \to 3$ contributions, and the total $\mathcal{O}(\alpha^3)$ cross section. The solid line represents the Born cross section.

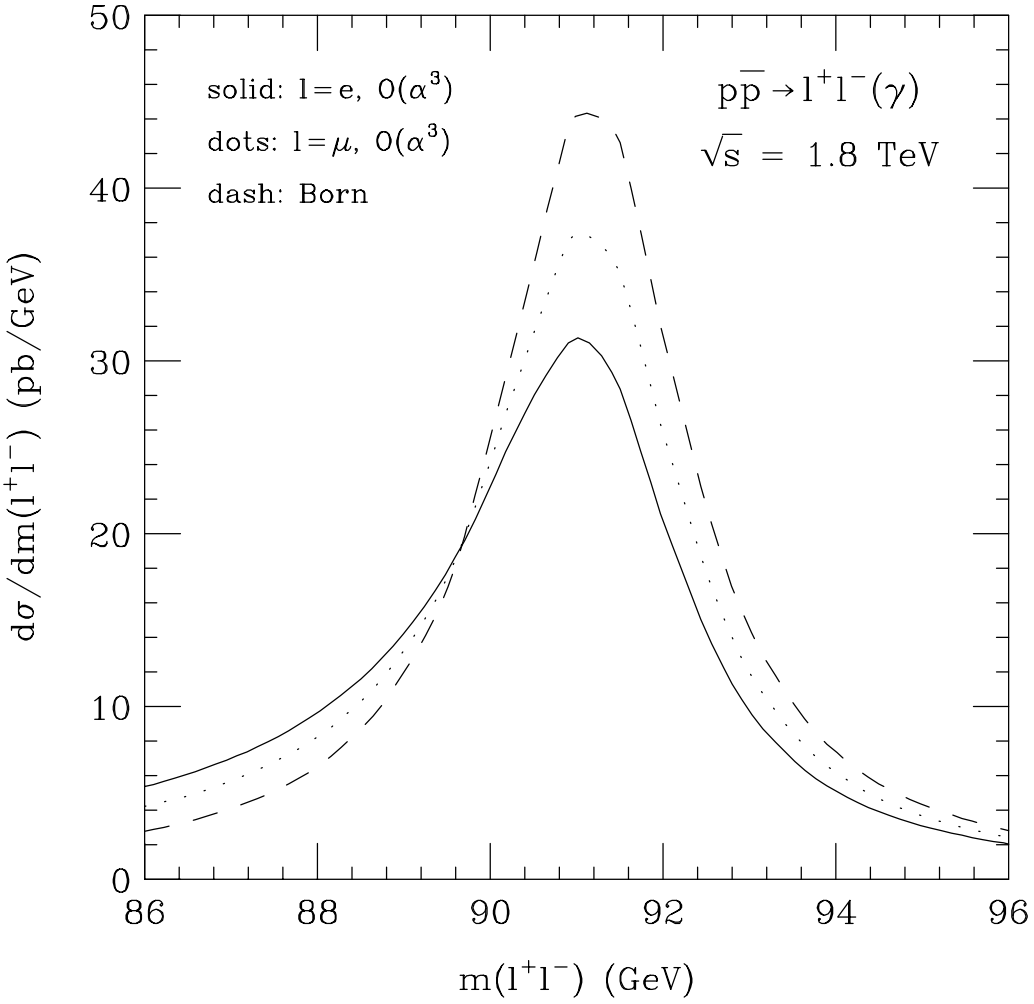

FIG. 3. The lepton pair invariant mass distribution for $p\bar{p} \to \ell^+\ell^-(\gamma)$ at $\sqrt{s} = 1.8$ TeV in the vicinity of the Z peak. The solid (dotted) line shows $d\sigma/dm(\ell^+\ell^-)$ for electron (muon) final states including $\mathcal{O}(\alpha)$ QED corrections. The dashed lines gives the $\ell^+\ell^-$ Born cross section.

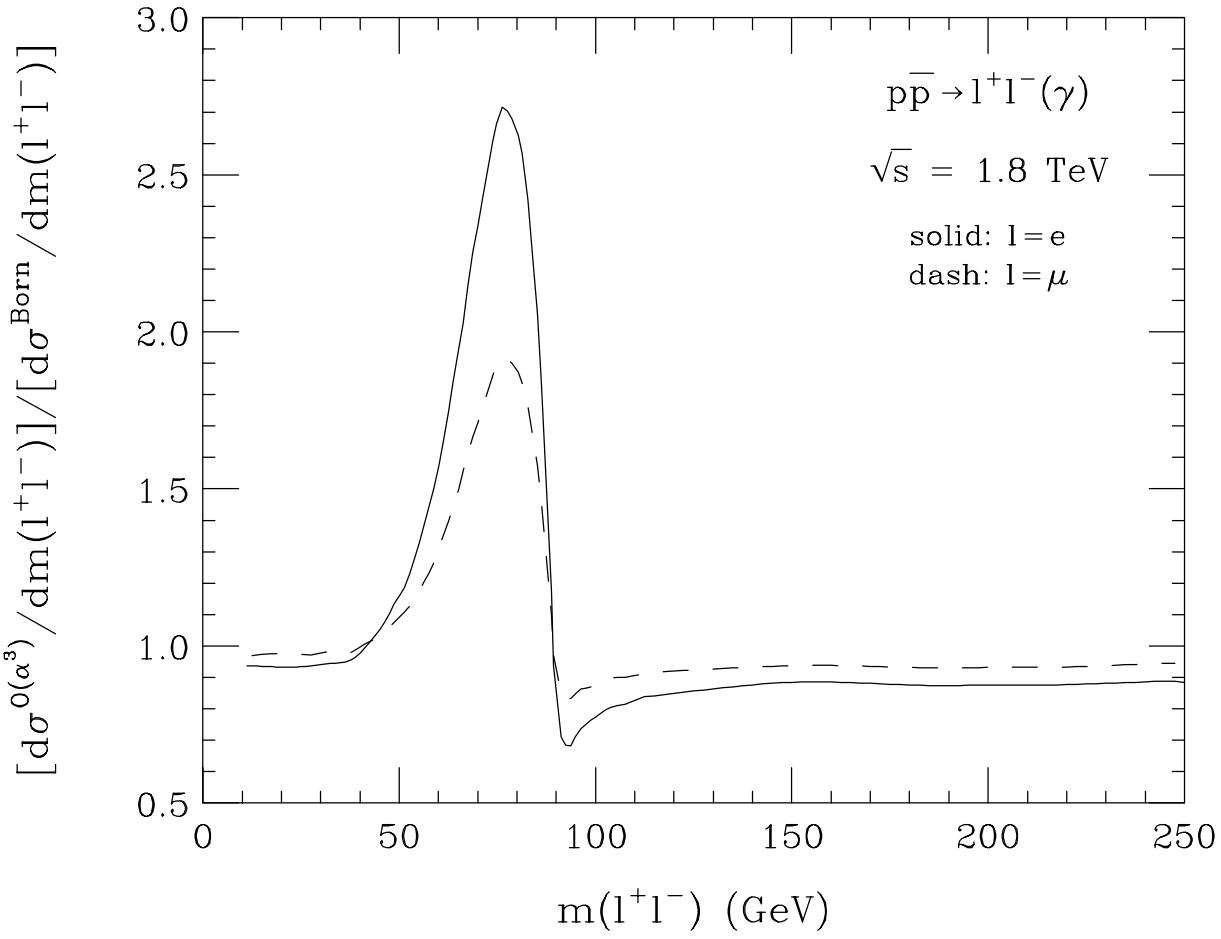

FIG. 4. Ratio of the $\mathcal{O}(\alpha^3)$ and lowest order differential cross sections as a function of the di-lepton invariant mass for $p\bar{p} \to \ell^+\ell^-(\gamma)$ at $\sqrt{s} = 1.8$ TeV. The solid line shows the result obtained for final state electrons, whereas the dashed line displays the cross section ratio for muons.

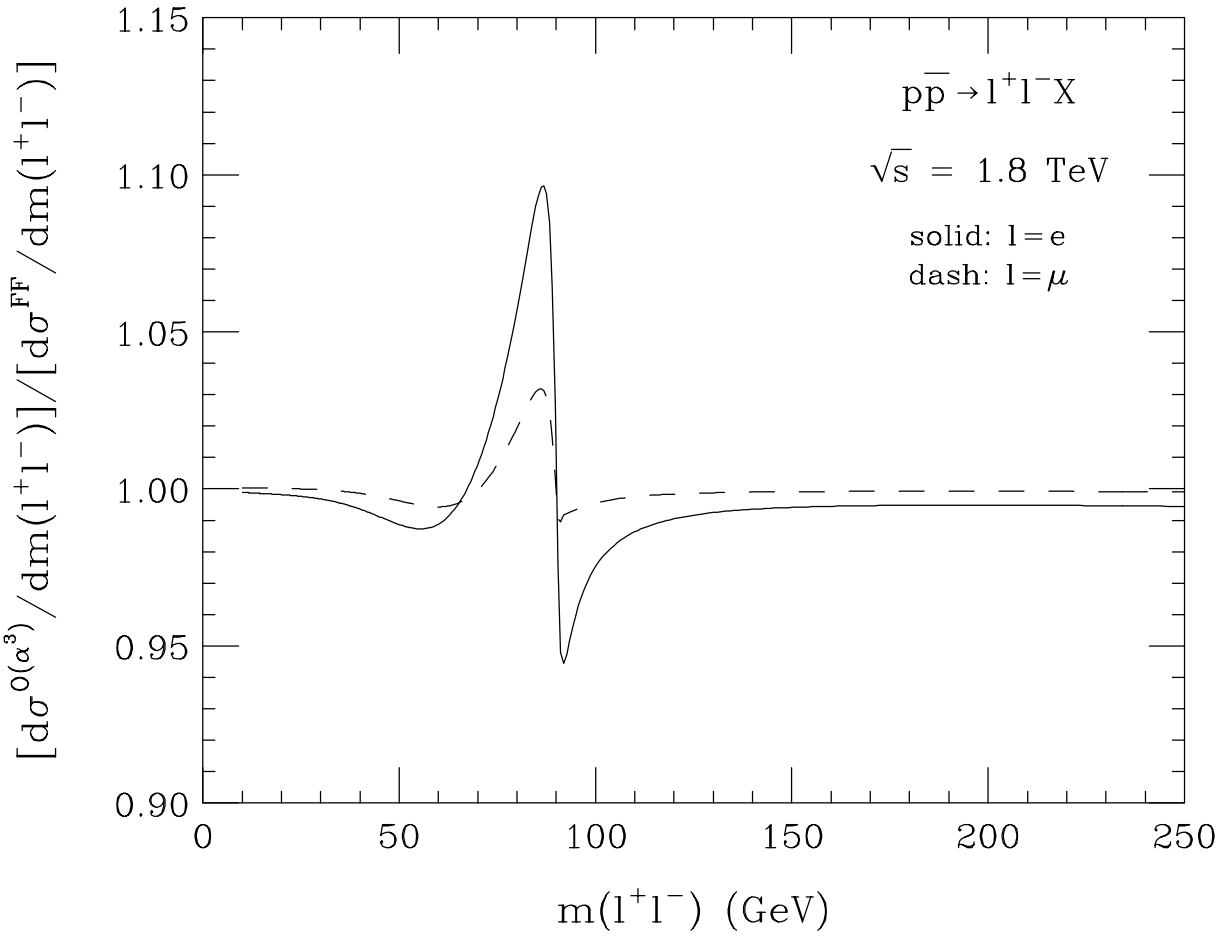

FIG. 5. Ratio of the $\mathcal{O}(\alpha^3)$ cross section and the cross section obtained in the fragmentation function approach (σ^{FF}) as a function of the di-lepton invariant mass for $p\bar{p} \to \ell^+\ell^- X$ at $\sqrt{s} = 1.8$ TeV. The solid line shows the result obtained for final state electrons, whereas the dashed line displays the cross section ratio for muons. In the fragmentation function approach, only final state corrections are taken into account.

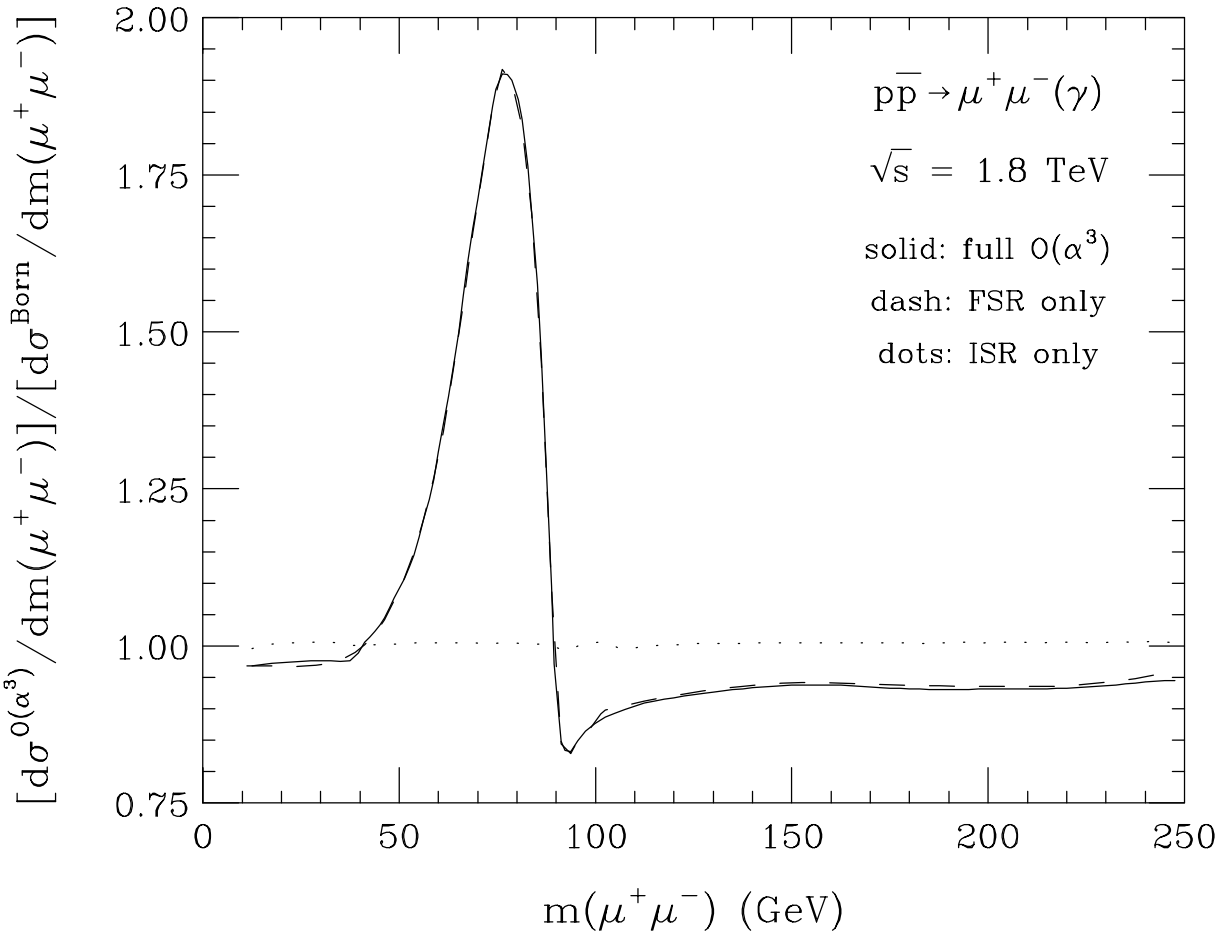

FIG. 6. Ratio of the $\mathcal{O}(\alpha^3)$ and lowest order differential cross sections as a function of the di-muon invariant mass for $p\bar{p} \to \mu^+\mu^-(\gamma)$ at $\sqrt{s} = 1.8$ TeV. The solid line gives the result for the full set of $\mathcal{O}(\alpha^3)$ QED diagrams. The dashed and dotted lines show the ratio obtained taking only final state and initial state corrections, respectively, into account.

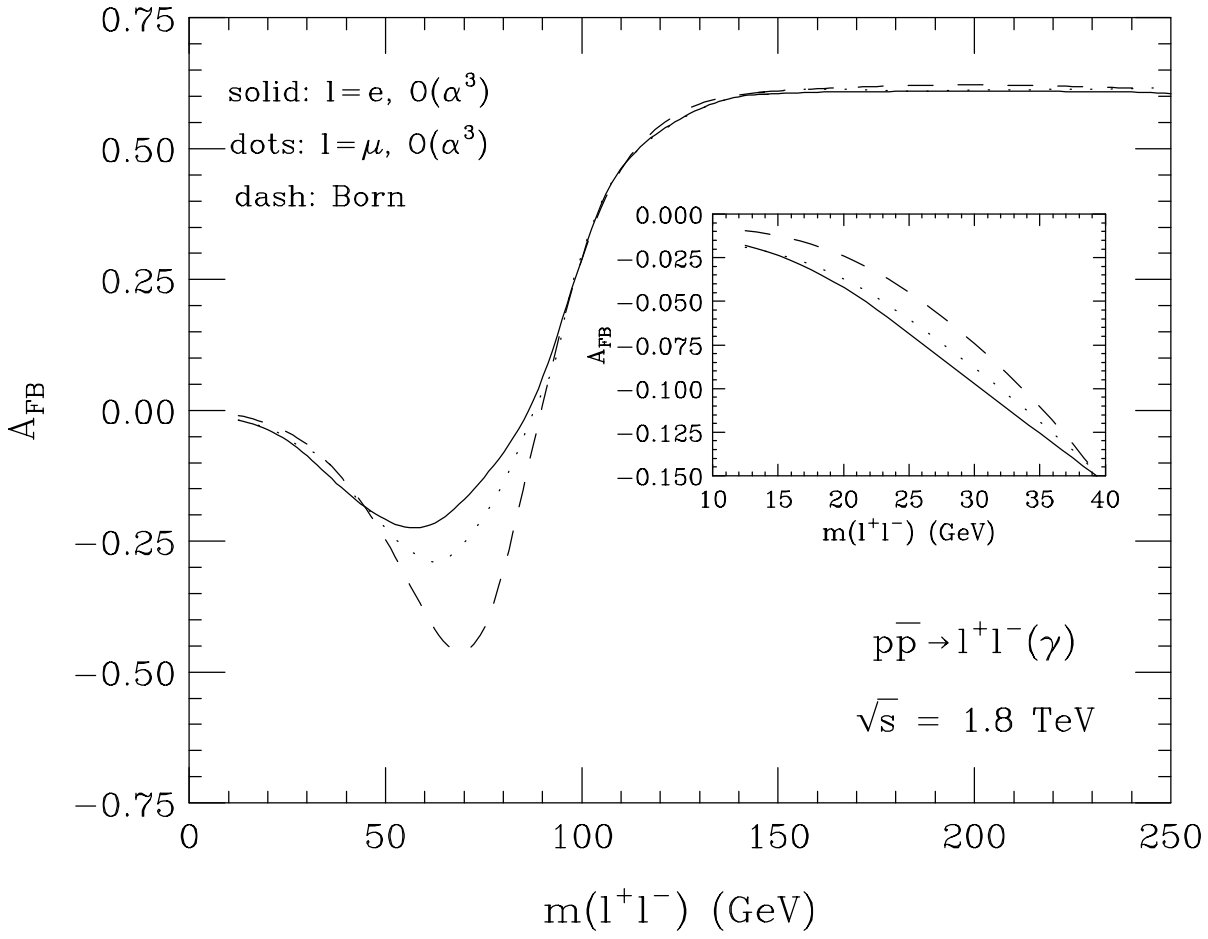

FIG. 7. The forward backward asymmetry, A_{FB}, as a function of the di-lepton invariant mass for $p\bar{p} \to \ell^+\ell^-(\gamma)$ at $\sqrt{s} = 1.8$ TeV. The solid and dotted lines show the forward backward asymmetry including $\mathcal{O}(\alpha)$ QED corrections for electrons and muons, respectively. The dashed line displays the lowest order prediction of A_{FB}. The inset provides a closeup of A_{FB} in the low mass region.

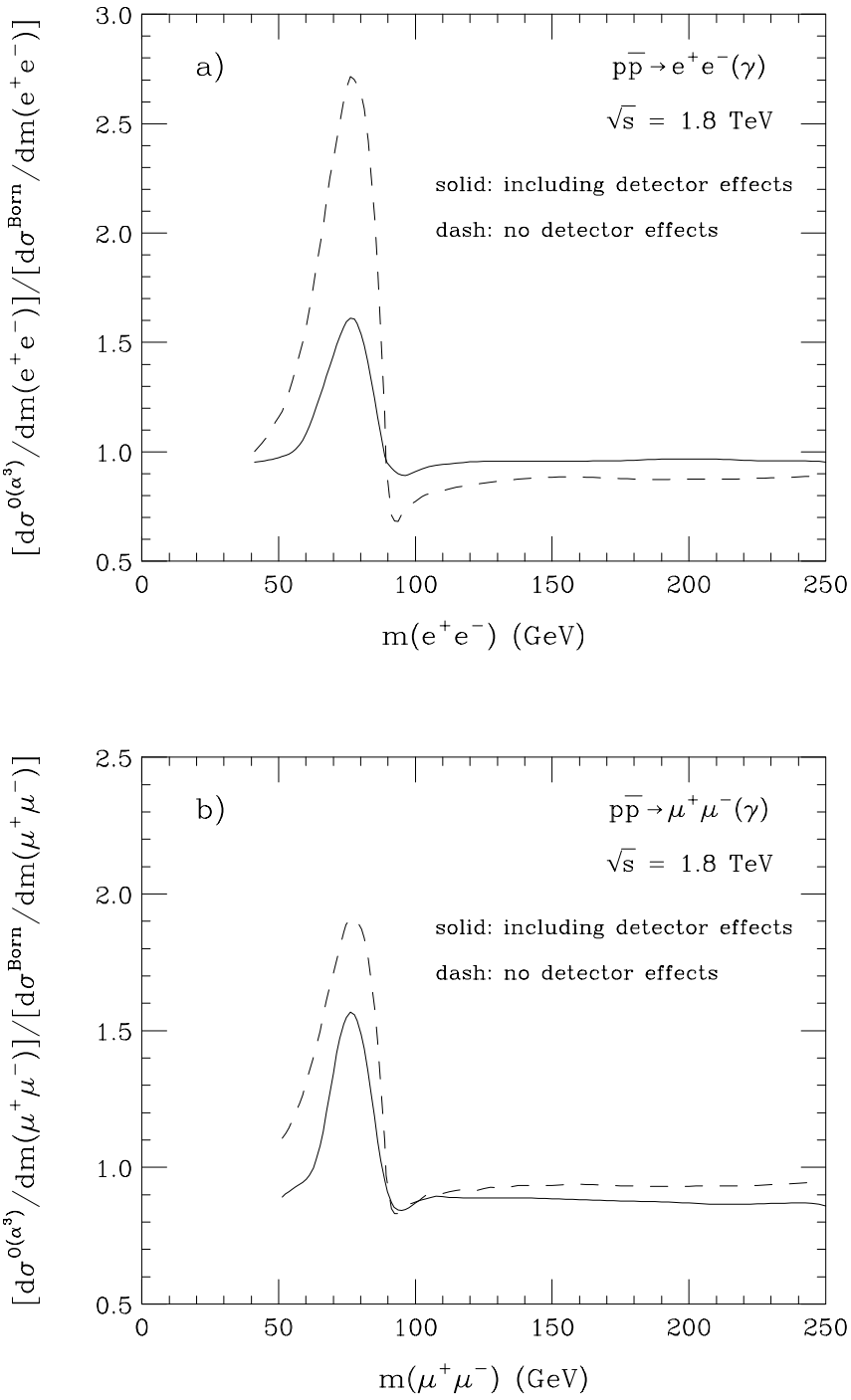

FIG. 8. Ratio of the $\mathcal{O}(\alpha^3)$ and lowest order differential cross sections as a function of the di-lepton invariant mass for a) $p\bar{p} \to e^+e^-(\gamma)$ and b) $p\bar{p} \to \mu^+\mu^-(\gamma)$ at $\sqrt{s} = 1.8$ TeV. The solid (dashed) lines show the cross section ratio with (without) the detector effects described in the text.

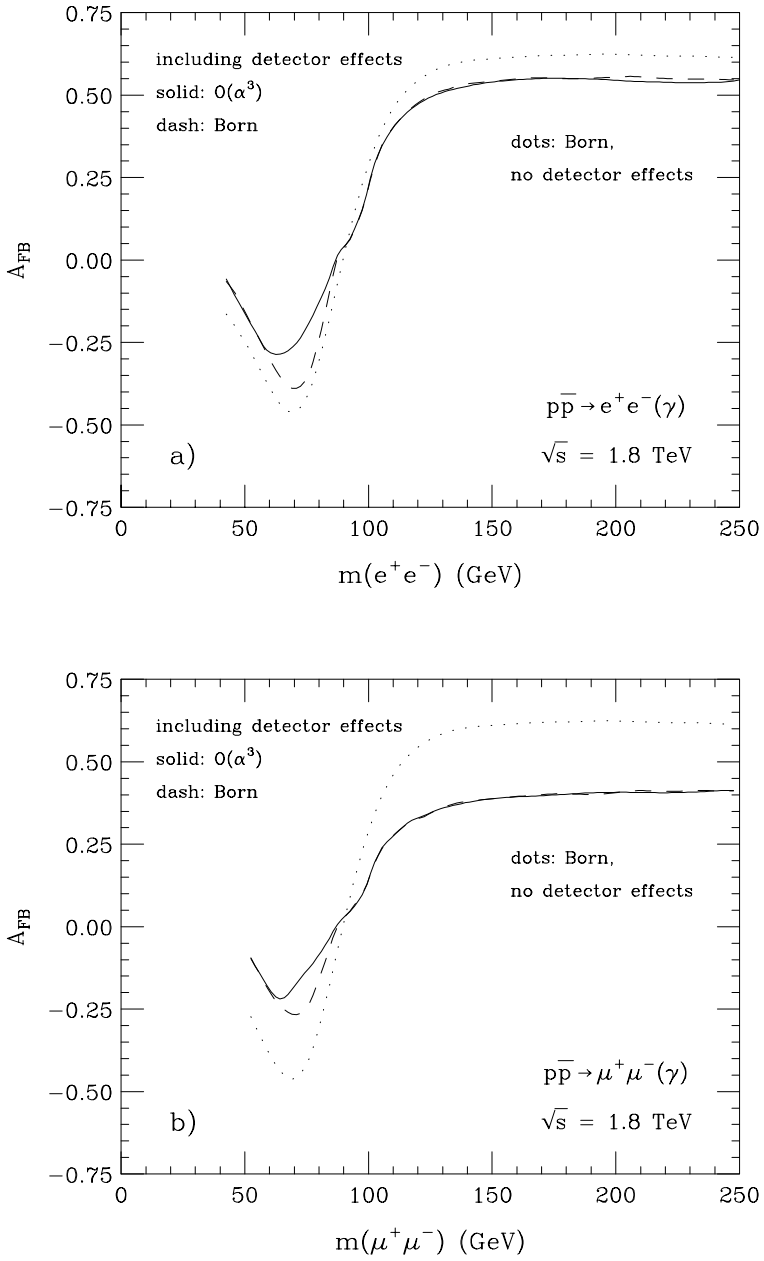

FIG. 9. The forward backward asymmetry, A_{FB}, a) for $p\bar{p} \to e^+e^-(\gamma)$ and b) for $p\bar{p} \to \mu^+\mu^-(\gamma)$ at $\sqrt{s} = 1.8$ TeV as a function of the di-lepton invariant mass. The solid lines show the result of the $\mathcal{O}(\alpha^3)$ calculation including detector effects (see text for details). The dashed and dotted lines represent the forward backward asymmetry in the Born approximation with and without detector effects.

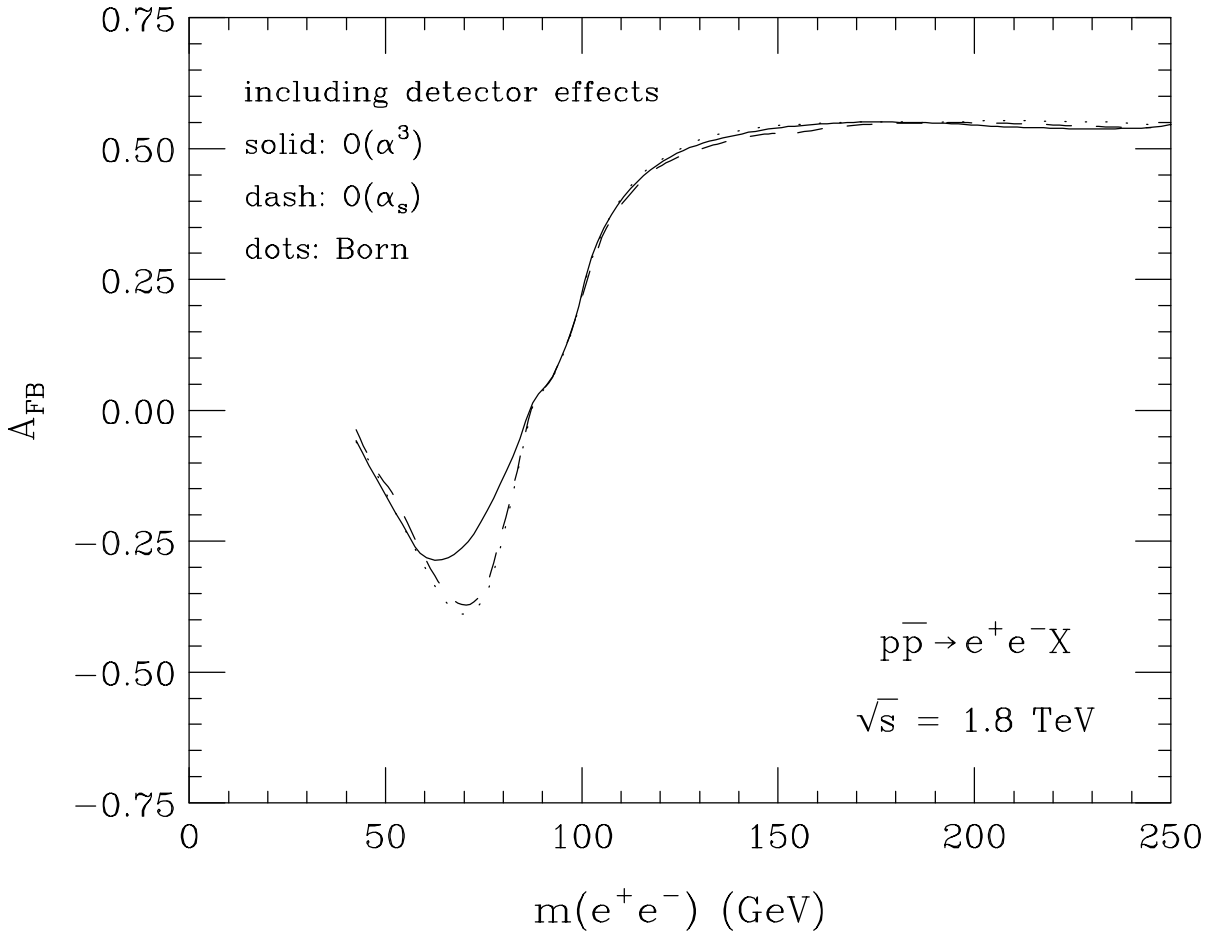

FIG. 10. The forward backward asymmetry, A_{FB}, including detector effects (see text for details) as a function of the e^+e^- invariant mass for $p\bar{p} \to e^+e^-X$ at $\sqrt{s} = 1.8$ TeV. The curves are for the forward backward asymmetry in the Born approximation (dotted line), including $\mathcal{O}(\alpha)$ QED corrections (solid line), and including $\mathcal{O}(\alpha_s)$ QCD corrections (dashed line).

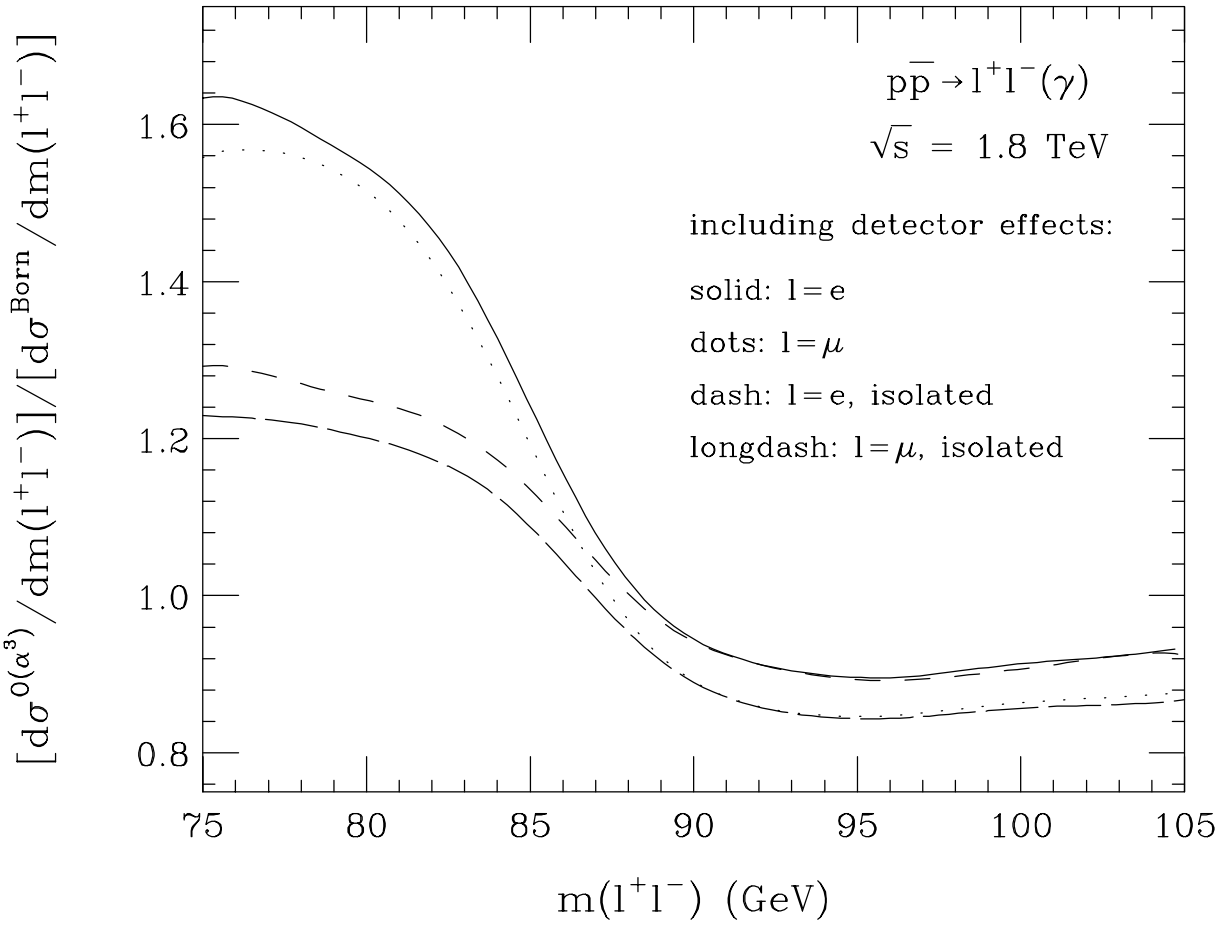

FIG. 11. Ratio of the $\mathcal{O}(\alpha^3)$ and lowest order differential cross sections, including detector effects (see text for details), as a function of the di-lepton invariant mass for $p\bar{p} \to \ell^+\ell^-(\gamma)$ at $\sqrt{s} = 1.8$ TeV in the Z peak region. The solid and dotted lines show the cross section ratio without imposing a lepton isolation cut for electrons and muons, respectively. The short-dashed and long-dashed lines give the result imposing in addition the isolation requirement of Eq. (23) with $R_0 = 0.4$ and $\epsilon_E = 0.1$.

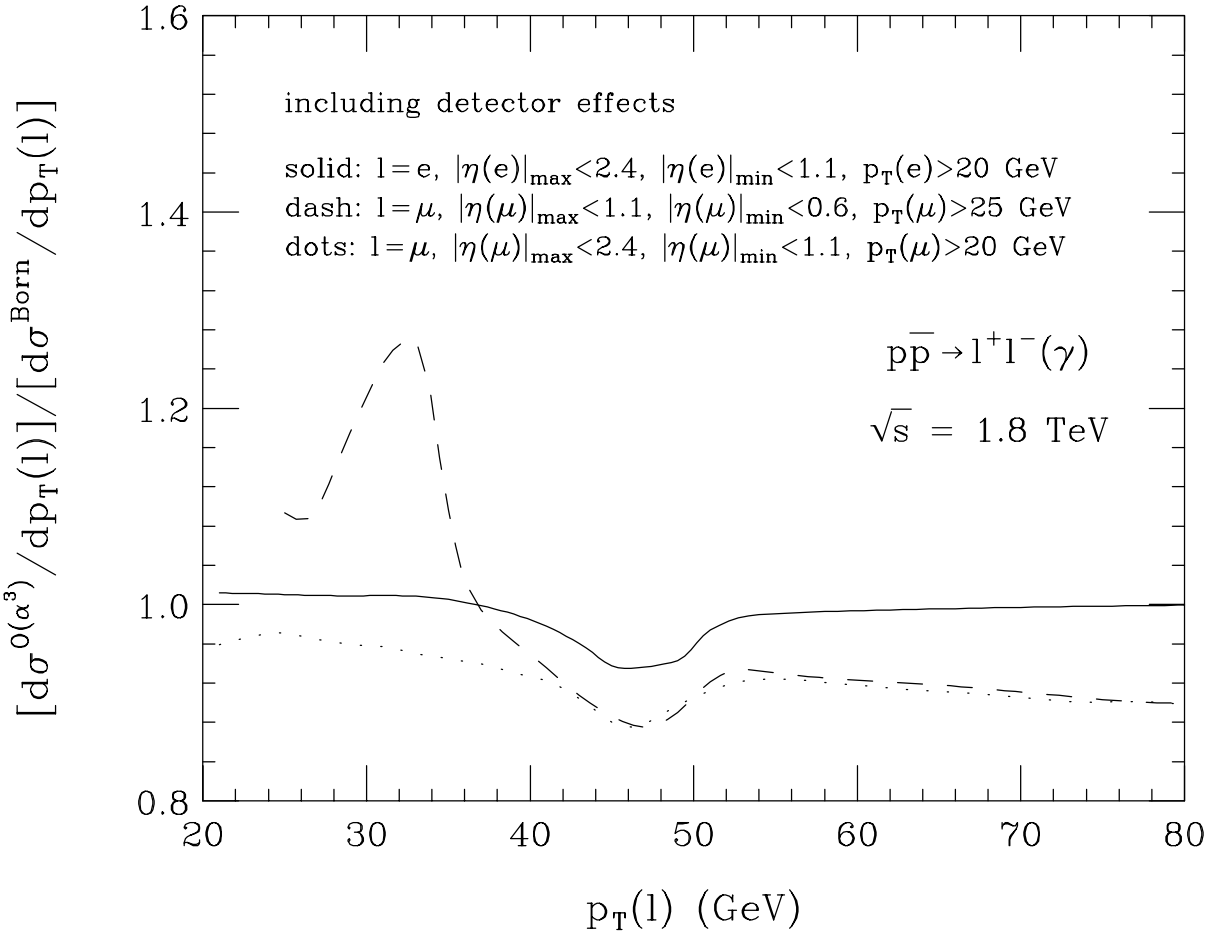

FIG. 12. Ratio of the $\mathcal{O}(\alpha^3)$ and lowest order differential cross sections, including detector effects (see text for details), as a function of the lepton transverse momentum in the reaction $p\bar{p} \to \ell^+\ell^-(\gamma)$ at $\sqrt{s} = 1.8$ TeV. The solid and dashed lines show the cross section ratio for electrons and muons, respectively, employing the acceptance cuts listed in the text. The dotted line displays the results for muons if the same pseudorapidity and p_T cuts as for electrons are used [$|\eta(\ell)|_{\rm max} = \max(|\eta(\ell^+)|, |\eta(\ell^-)|)$; $|\eta(\ell)|_{\rm min} = \min(|\eta(\ell^+)|, |\eta(\ell^-)|)$].

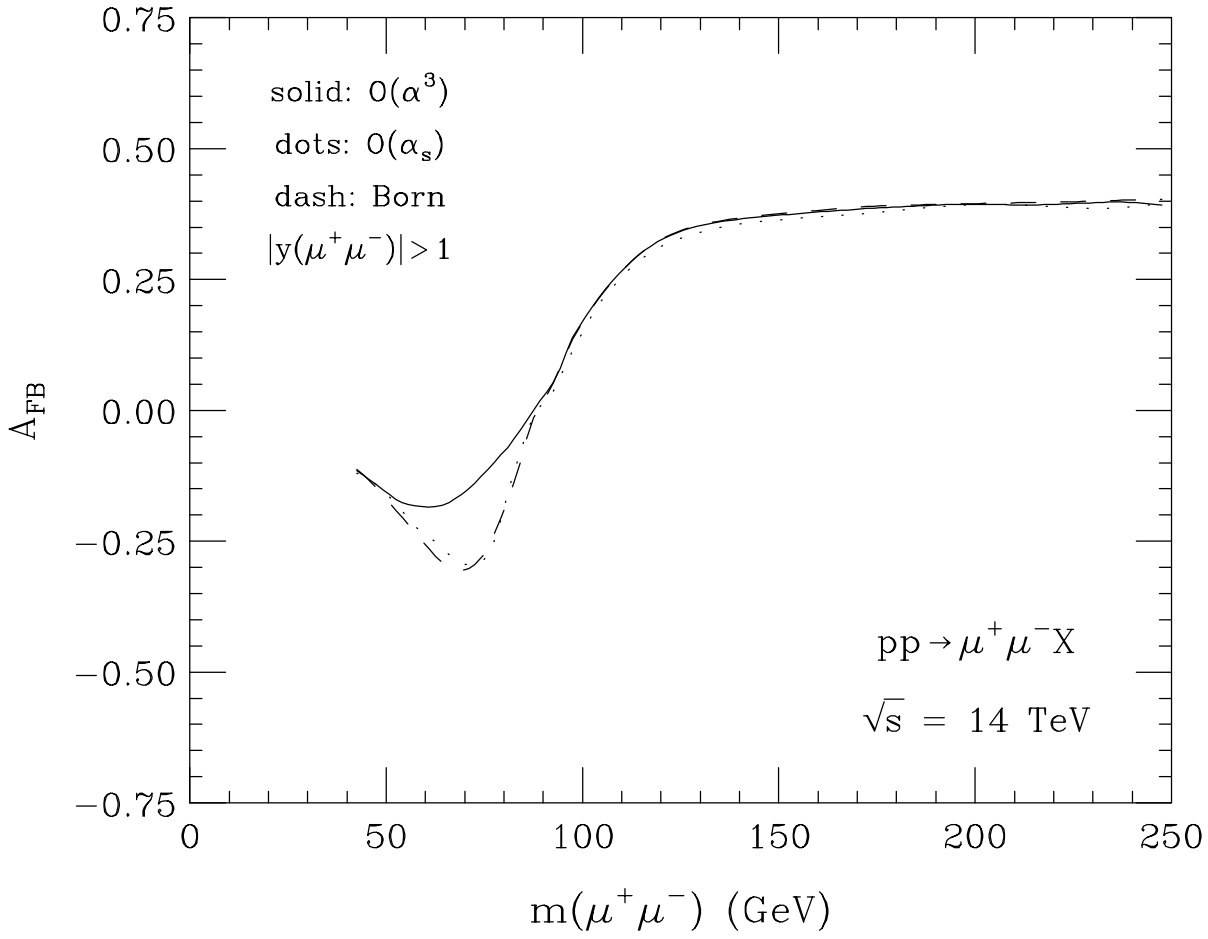

FIG. 13. The forward backward asymmetry, A_{FB}, as a function of the $\mu^+\mu^-$ invariant mass for $pp \to \mu^+\mu^-(\gamma)$ at $\sqrt{s} = 14$ TeV. The solid and dotted lines show the forward backward asymmetry including $\mathcal{O}(\alpha)$ QED and $\mathcal{O}(\alpha_s)$ QCD corrections, respectively. The dashed line displays the lowest order prediction of A_{FB}. A $|y(\mu^+\mu^-)| > 1$ cut is imposed on the rapidity of the muon pair. No detector effects are included here.

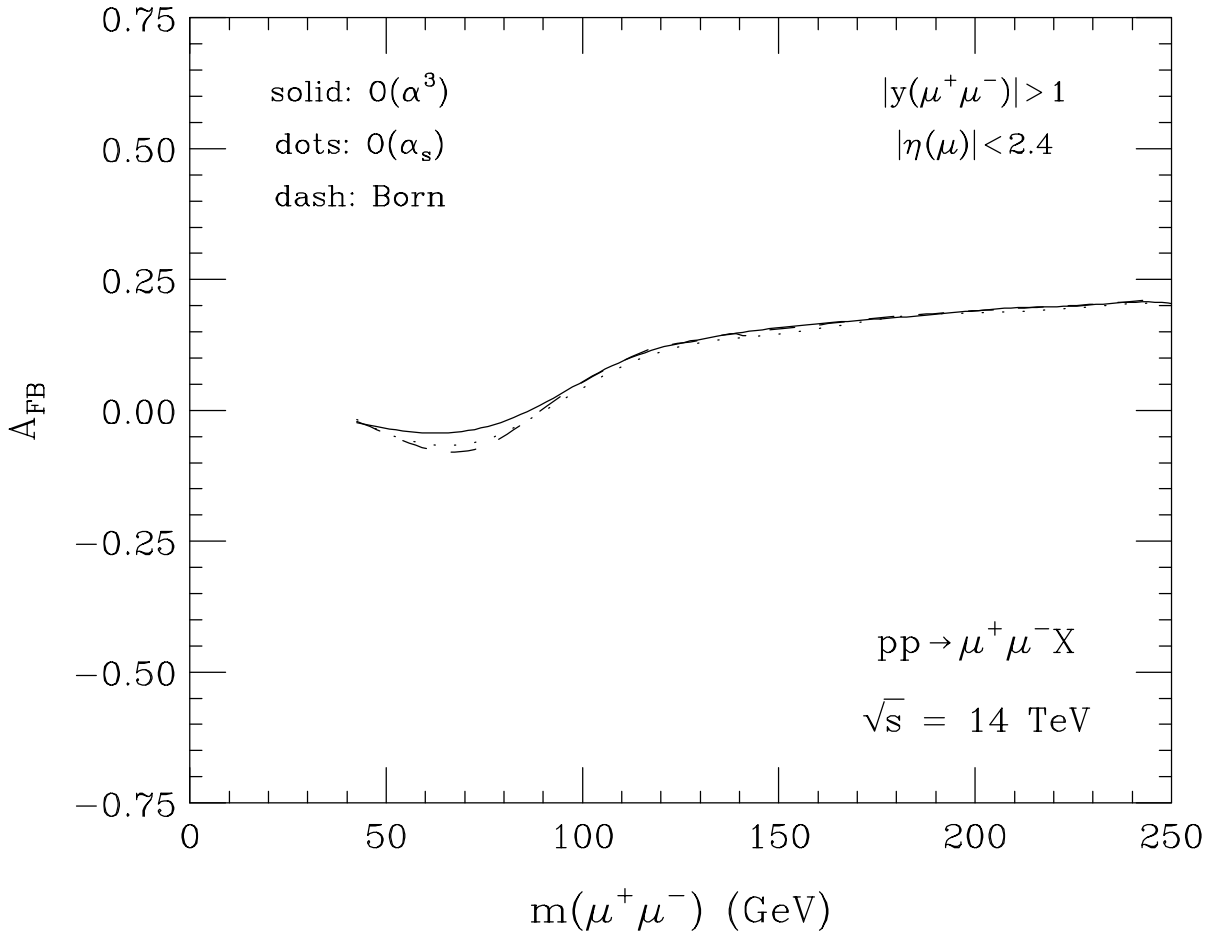

FIG. 14. The forward backward asymmetry, A_{FB}, as a function of the $\mu^+\mu^-$ invariant mass for $pp \to \mu^+\mu^-(\gamma)$ at $\sqrt{s} = 14$ TeV. A $|\eta(\mu)| < 2.4$ cut is imposed in addition to the $|y(\mu^+\mu^-)| > 1$ cut. The solid and dotted lines show the forward backward asymmetry including $\mathcal{O}(\alpha)$ QED and $\mathcal{O}(\alpha_s)$ QCD corrections, respectively. The dashed line displays the lowest order prediction of A_{FB}.